



UNIVERSITY OF LATVIA

DEPARTMENT OF PHYSICS AND MATHEMATICS

INSTITUTE OF SOLID STATE PHYSICS

JELENA BUTIKOVA

**LASER ABLATION SPECTROSCOPY FOR IMPURITY DEPTH
PROFILING IN HOT WALL MATERIALS OF THERMONUCLEAR
FUSION REACTORS**

Doctoral thesis

Scientific supervisor: Dr. habil. phys. Ivars Tāle

RIGA

2009



LATVIJAS UNIVERSITĀTE

**FIZIKAS UN MATEMĀTIKAS FAKULTĀTE
CIETVIELU FIZIKAS INSTITŪTS**

JEĻENA BUTIKOVA

**PIEMAIŠĪJUMU SADALĪJUMA LĀZERABLĀCIJAS SPEKTROSKOPIJA
KODOLSINTĒZES REAKTORU KARSTĀS SIENAS MATERIĀLU
DIAGNOSTIKAI**

Promocijas darbs

**doktora grāda iegūšanai fizikas nozarē
cietvielu fizikas apakšnozarē**

Zinātniskais vadītājs: Dr. habil. phys. Ivars Tāle

RĪGA

2009

ABSTRACT

This thesis comprises 88 pages, 31 figures and 2 tables. The thesis consists of 4 parts. The thesis contains 111 references on scientific papers.

Keywords: LASER ABLATION, PLASMA PRODUCTION AND HEATING BY LASER BEAMS, LASER-BEAM IMPACT PHENOMENA

The main motivation of this study was to show the efficiency of the laser-induced ablation for analysis of the impurities in plasma facing components as the method allows the detection of any chemical element and can be employed for the remote analysis. This is an essential moment for the plasma facing materials as the detection of the hydrogen isotopes and detritiation is one of the crucial tasks for the analysis of the surface of the plasma facing components, and because of their irregular shapes forming spaces which are difficult to reach.

The major tasks of the present investigation are setting up and testing the equipment for laser ablation spectroscopy and developing the methodology for impurity depth profiling.

The thesis describes the investigation of the samples of ASDEX Upgrade divertor plates by means of laser-induced ablation spectroscopy and profilometry of the corresponding ablation craters. The results obtained from the Rutherford backscattering spectroscopy of these plasma facing materials are also mentioned. These data was obtained in co-operation with the Max-Planck-Institut für Plasmaphysik (Garching, Germany).

The experimental set-up for the laser-induced ablation spectroscopy was developed and partly manufactured at the Institute of Solid state Physics. The design of the vacuum chamber used in the investigation is described in the thesis.

Laser-induced plasma emission spectra of the ASDEX Upgrade divertor samples were obtained using a Nd:YAG 1064 nm laser with pulse length of 150 ps and repetition rate of 10 Hz. The spectra of the ASDEX Upgrade samples show a substantial number of impurities. The impurities were determined, and the possible sources of the impurities suggested.

Laser-induced ablation was performed at different pressure values in the vacuum chamber. The pressure of 10^{-5} Torr is decided to be the optimal as the spectra taken at this value is well resolved and exhibit the maximal amount of lines among the other pressure values used for the investigations. The spectral lines of the impurities of interest are not subjected to the broadening as pronounced as it is in the case of the experiments at the atmospheric pressure. Moreover, the pressure of 10^{-5} Torr is easier to sustain technically during the experiments.

Registration of the emission spectra at various distances from the target was performed. The results show that selective detection of the plasma light might improve signal-to-noise ratio in the spectra reducing strong background continuum occurring at early stages of plasma formation without time-resolved detection.

The evolution of the signals of the impurities was observed applying several laser pulses onto the same spot of the ablated sample and recording the emission spectrum after each signal. Considering the ablation removal rate, the results obtained for low pressure values correspond to those obtained during the measurements at atmospheric pressure. Almost all the deuterium found in the ASDEX Upgrade samples is released from the depth of 0.5-1 μm inside the bulk material. The concentration of boron is maximal 1 μm in the surface, and then the concentration decreases.

The obtained results allows considering the method of the laser-induced ablation spectroscopy to be feasible for rapid analysis of plasma facing materials. With minor modifications, this method can be suggested as an *in situ* technique for determination the state of the plasma facing components inside the chamber of a thermonuclear fusion reactor.

This thesis is structured in four chapters followed by the conclusions and perspectives. Chapter 1 includes the basic principles of the laser-induced ablation spectroscopy. Several theoretical approaches and models are described. Also, an overview of plasma-wall interaction is given. Chapter 2 is an overview of the literature. Chapter 3 describes the experimental details of the investigations, and chapter 4 part comprises the results and discussion. Finally, the list of scientific contributions which I participated in is included.

Anotācija

Disertācijā ir 88 lpp., 31 zīmējumi un 2 tabulas. Disertācija sastāv no četrām daļām. Literatūras sarakstā iekļautas atsauces uz 111 zinātniskiem darbiem.

Atslēgas vārdi: LĀZERA ABLĀCIJA, PLAZMAS VEIDOŠANA UN SILDĪŠANA AR LĀZERA STARIEM, LĀZERA STARU IEDARBĪBAS PARĀDĪBAS

Promocijas darba galvenā motivācija ir parādīt lāzerinducētās ablācijas spektroskopijas metodes efektivitāti plazmu skarošo materiālu piemaisījumu analīzei, jo šī metode ļauj noteikt jebkuru ķīmisko elementu materiālā un var tikt izmantota kā tālvadāmā analīzē. Šie aspekti ir ļoti būtiski, jo ūdeņraža izotopu detektēšana un detritiācija ir izšķiroši uzdevumi plazmu skarošo komponentu virsmas analīzē, kā arī tāpēc, ka komponentu neregulārās formas veido grūti sasniedzamās telpas.

Promocijas darba mērķis ir izpētīt ASDEX Upgrade tokamaka plazmu skarošā materiāla ar lāzerablācijas spektroskopijas metodi, parādot piemaisījumu sastāvu tajā, kā arī dziļumu, kurā tiek akumulēti svarīgākie piemaisījumu elementi – ūdeņradis un bors.

Promocijas darba pamatuzdevumi ir uzstādīt un palaist iekārtu lāzerablācijas spektroskopijas mērījumiem, kā arī izstrādāt metodiku piemaisījumu dziļuma sadalījuma noteikšanai.

ASDEX Upgrade tokamaka divertora plāksņu paraugi tika analizēti izmantojot lāzerablācijas spektroskopijas metodi. Ablācijas krāteri, kas izveidojās pētīšanas procesā, tika pētīti ar profilometrijas palīdzību. Pētāmo paraugu Rezerforda atpakaļizkliedes spektroskopijas rezultāti arī tiek minēti šajā darbā. Šie dati tika iegūti sadarbībā ar Maksa Planka Plazmas fizikas institūtu (Garhinga, Vācija).

Eksperimentālā iekārta lāzerablācijas spektroskopijas mērījumiem tika izstrādāta un daļēji izgatavota Latvijas Universitātes Cietvielu Fizikas institūtā. Vakuuma kameras konstrukcija ir aprakstīta promocijas darba eksperimentālajā daļā.

ASDEX Upgrade divertora paraugu lāzerinducētās plazmas emisijas spektri tika iegūti ar Nd:YAG lāzera palīdzību. Izmantotā 1064 nm viļņa garuma impulsa garums bija 150 ps, frekvence – 10 Hz.

ASDEX Upgrade paraugu spektri parāda lielu piemaisījumu skaitu. Piemaisījumu elementi tika identificēti, un ierosinot to iespējamus avotus.

Lāzerinducēto ablāciju spektru mērīšana notika vakuuma kamerā pie dažādām spiediena vērtībām. Tika konstatēts, ka 10^{-5} Torr spiediens ir optimāls šiem mērījumiem, jo pie šīs vērtības iegūtie spektri ir labi izšķirti un demonstrē maksimālo spektrālo līniju skaitu salīdzinot ar citām spiediena vērtībām, kas tika izmantoti pētījumos. Ūdeņraža un bora spektrālās līnijas netika pakļauti paplašinājumam tik spēcīgi, kā tas notika eksperimentos pie atmosfēras spiediena. Turklāt, 10^{-5} Torr spiedienu var tehniski ērtāk uzturēt eksperimenta laikā.

Plazmas emisijas spektri tika reģistrēti dažādos attālumos no parauga virsmas. Rezultāti rāda, ka plazmas gaismas selektīva detektēšana var uzlabot signāla-trokšņa attiecību spektrā, samazinot nepārtraukta starojuma, kas rodas plazmas veidošanās agrīnajās stadijās, ietekmi. Šī ietekme ir būtiska, reģistrējot plazmas starojumu bez laika izšķiršanas.

Piemaisījumu elementu signālu evolūcija tika novērota iedarbojoties ar secīgajiem lāzera impulsiem uz parauga virsmas, nemainot ablācijas vietu. Signāls tika pierakstīts pēc katra impulsa. Salīdzinot ablētā materiāla daudzumu, var secināt, ka rezultāti, kas iegūti pie zemām spiediena vērtībām un pie atmosfēras spiediena, saskan. Gandrīz viss ūdeņradis, kas atrasts ASDEX Upgrade paraugos, tiek izlaists ar lāzera stara iedarbību no 0.5-1 μm dziļuma. Bora koncentrācija sasniedz maksimālo vērtību 1 μm dziļumā, samazinoties līdz ar ablācijas krātera dziļums palielināšanos.

Iegūtie rezultāti ļauj secināt, ka lāzerinducētās ablācijas spektroskopijas metode ir atbilstoša plazmu skarošo materiālu ekspresanalīzei. Ar nelielajām modifikācijām šo metodi var pielietot kā *in situ* tehniku plazmu skarošo komponentu stāvokļa apsekošanu kodoltermiskās sintēzes reaktora kamerā.

Promocijas darba pirmā daļa stāsta par lāzerablācijas spektroskopijas pamatprincipiem. Tika aprakstīti dažas teorētiskas pieejas un modeļi. Ir apskatītas arī plazmas un reaktora sienas mijiedarbība kodoltermiskās sintēzes reaktora kamerā. Otrā daļa satur konspektīvu literatūras apskatu. Trešajā daļā aprakstīti pētāmie paraugi un eksperimenta metodika. Ceturtajā daļā apkopoti iegūtie rezultāti.

Content

Abstract	3
Anotācija	5
Introduction	8
1.1. Physical processes in pulsed laser ablation	11
1.1.1 Light-material interaction	12
1.1.2 Removal of Target Material	14
1.2.1.1 Ablation	15
1.1.3. Gas and plasma dynamics	17
1.2. Plasma facing materials. Plasma-wall interaction	20
1.2.1 Hydrogen fuel cycle	22
1.2.1.1 Reflection	23
1.2.1.2 Implantation, diffusion and re-emission	23
1.2.2 Methods of impurity production	24
1.2.2.1 Sputtering	25
1.2.2.2 Desorption	26
1.2.2.3 Evaporation and sublimation	26
1.2.2.4 Arching and melting	27
1.2.2.5 Chemical reactions	27
1.2.3 Minimizing impurities	28
1.2.3.1 Vessel conditioning	28
1.2.3.2 Impurity screening	28
1.2.3.3 Materials selection	28
2. Overview on the literature	30
2.1 Laser-induced ablation spectroscopy	30
2.2 Plasma facing materials	33
3. Experimental techniques	37
3.1 Nd:YAG laser	37
3.2 Vacuum chamber	40
3.3 Target materials	42
3.4 Target holders	43
3.5 Plasma detection equipment	44
3.6 Rutherford backscattering spectroscopy	44
3.7 Profilometry	45
4. Results and discussion	46
4.1 Ablation in air/atmospheric pressure	46
4.2 Ablation in vacuum	54
4.2.1 Ablation at different pressure values	54
4.2.2 Registration of emission spectra at various distances from the target	59
4.2.3 Ablation at different pulse energies. Depth profiles	62
Theses	69
Conclusions and perspectives	70
References	73
List of author's scientific publications	85
Participation in conferences	86
Acknowledgments	88
Appendix	

Introduction

The primary requirement for generation of power from thermonuclear fusion reactions is that the energy input needed to sustain the plasma conditions be less than the energy output gained from these reactions. The implementation of this goal depends on two physical conditions accomplished in the reactor simultaneously. One is that the plasma should be maintained at the temperature high enough to ignite the fuel. The other one is that the plasma must be contained at sufficiently high densities for a certain period of time called confinement time to ensure the loads of nuclear reaction to occur [1].

The topicality of the research theme

The main issue for design and construction of a thermonuclear fusion reactor with magnetically confined plasma is the interaction of the hot plasma with the material components of such a device. Plasma facing components of a vessel act as a reservoir for energy and particles coming from the plasma. In the same time, the particle interaction with the surface of the material surface may cause the wall atoms and the atoms implanted from the fuel to release and to enter the plasma.

One of the main problems caused by the processes of plasma interaction with reactor wall materials is contamination of the plasma by impurities released from the vessel components. Impurities can interact strongly with plasma to emit high-energy radiation causing a cooling of plasma below the ignition temperature. An additional problem is the alteration of the material structure by the particle bombardment and the high energy flux which may limit the lifetime of the plasma facing components significantly. These problems must be solved under the constraint that the generated power has to pass through the vessel components at some location. The wall may further act as a reservoir for the hydrogen fuel isotopes leading to an uncontrollable additional source of fuel atoms, which may cause problems in maintaining stationary discharge conditions [1, 2].

Goals and motivation of the work

The optimal plasma facing material for future fusion devices is still not found. The choice of materials for plasma facing components in a fusion reactors are determined by the plasma interaction with these materials. The most important aspects in terms of safety as well as economics

of the future fusion devices concerns the lifetime of plasma facing components and deuterium/tritium inventory problem. Various surface diagnostic methods are employed to study the processes caused by the plasma-material interaction. Ion beam techniques [3, 4], ion probes [5], laser-induced fluorescence [6], interference fringe analysis [7], ellipsometry [8], X-ray photoelectron spectroscopy and thermal desorption spectroscopy [9], laser interferometry and fast photography [10] are among them.

In comparison to the mentioned techniques, there are certain advantages of laser-induced ablation spectroscopy. It is virtually non-destructive analysis of any material since only a tiny amount of material is consumed during the process. Heating of the sample is negligible. In principle, the method of laser ablation spectroscopy allows performing elemental analysis of any material, irrespective of its physical state.

No sample preparation is necessary for this method. Laser ablation spectroscopy allows analysing a material directly without the need to prepare the sample beforehand. Should the sample material be coated with another material, the laser radiation may be used to first clean the surface of the sample in order to expose the underlying material to allow chemical analysis to be carried out. The efficiency of the laser cleaning process depends upon the type of material being removed and the power of the laser. The acoustic shock-wave of the laser plasma is particularly effective at removing semi-liquid or viscous materials.

One of the most important advantages of the laser ablation spectroscopy which is particularly important for the treatment of plasma facing components is the possibility of remote analysis of the material using this technique. With this method, a certain regions in a tokamak which are difficult to reach, such as gaps [11] or castellated structures [12], can be analysed remotely.

The main motivation of this study was to show the efficiency of the laser-induced ablation for analysis of the impurities in plasma facing components as the method allows the detection of any chemical element and can be employed for the remote analysis. This is an essential moment for the plasma facing materials as the detection of the hydrogen isotopes and detritiation is one of the crucial tasks for the analysis of the surface of the plasma facing components, and because of their irregular shapes forming spaces which are difficult to reach.

The goal of the study was to investigate plasma facing material of the ASDEX Upgrade tokamak using the method of laser ablation spectroscopy showing the impurity content in given plasma facing component, as well as the depth of the accumulation of the impurities of the major concern – that is, hydrogen and boron.

The major tasks of the present investigation are the following:

- setting up and testing the experimental equipment for the laser induced breakdown spectroscopy analysis of the plasma facing materials;
- developing the methodology of the laser ablation of impurity depth profiling;
- proving that the laser-induced ablation spectroscopy is a feasible technique for the rapid analysis of plasma facing materials with a perspective to develop *in situ* method of inspection the status of plasma facing materials inside the tokamak.

This thesis is structured in four chapters followed by the conclusions and perspectives. Chapter 1 includes the basic principles of the laser-induced ablation spectroscopy. Several theoretical approaches and models are described. Chapter 2 is an overview of the literature. Chapter 3 describes the experimental details of the investigations, and chapter 4 part comprises the results and discussion. Finally, the list of scientific contributions which I participated in is included.

Author's contribution

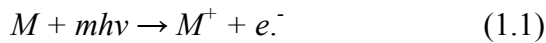
This study was performed in co-operation with several scientific collaborators. Author's contribution includes setting up and maintenance of the experimental equipment, performing measurements, data processing and summarizing.

The results of this study were discussed at the scientific seminar held on 17 September 2008 at the Institute of Solid State Physics, University of Latvia. The results were published in 5 articles and presented at 14 conferences.

1.1. Physical processes in pulsed laser ablation

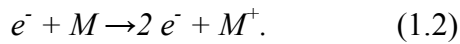
Laser-induced breakdown can be defined as the generation of a practically totally ionized gas (plasma) by the end of the laser pulse [13]. It can be observed experimentally as a glow or flash in the focal region. More quantitative criteria include measurements of attenuation of the laser beam and the level of ionization in the focal region.

Two main mechanisms for electron generation and growth can be described. The first one called multiphoton ionization (MPI) involves the simultaneous absorption by an atom or molecule a sufficient number of photons to eject an electron from valence to conduction band. It can be described by the reaction [13]



If ε_I is band gap, the number of photons m should exceed the integer part of $(\varepsilon_I/h\nu + 1)$.

The other mechanism works when electrons absorb laser radiation with they collide with neutrals. If electrons gain sufficient energy, they can ionize the matter by impact through the reaction



This leads to the cascade breakdown, or exponential growth of electron concentration in time. In this case, electrons gain energy in a process called inverse Bremsstrahlung (IBE). The electrical field induced by the laser causes electrons to oscillate. This oscillation energy is converted into thermal energy via electron-ion collision. Bremsstrahlung and IBE are connected the following way: if two charged particles undergo a Coulomb collision they emit radiation – so called Bremsstrahlung. IBE is an inverse process when an electron is scattered in the field of ion absorbs a photon. If the laser fluence is high enough, in spite of energy losses, some electrons will gain energy high enough to generate new electrons for cascade growth to take place. This process becomes more important for laser pulses with $\lambda > 1 \mu\text{m}$.

Multiphoton ionization is important for wavelength $\lambda < 1 \mu\text{m}$. For laser pulses with $\lambda > 1 \mu\text{m}$, IBE plays more significant role. However, both processes are important at any wavelength of the laser pulse as MPI can be a mechanism furnishing electrons for IBE [13].

1.1.1. Light-material interaction

The process of energy transfer from laser beam to material is very important in laser ablation. The interaction mechanism between laser light and matter mainly depends on the parameters of laser beam (wavelength, pulse duration and energy, repetition rate) and physical and chemical properties of the material.

When laser radiation is absorbed in a surface region of a solid target, the electromagnetic energy is converted into electronic excitation in the form of plasmons, unbound electrons and holes and, in the case of insulators and semiconductors, excitons. Under high excitation, the concentration of the excited carriers is also high and they can form an electron-hole plasma.

The laser source term couples directly into the electronic distribution, promoting the electrons into highly excited states. At high fluences, a large fraction of the electrons are promoted into antibonding orbitals. The covalent bonds are weakened and the interatomic forces changed by this process. The system responds to the local differences in bonding interaction by ‘melting’ without any appreciable energy transfer between the excited ions and the lattice. This process has been termed ‘plasma annealing’ and can explain the fast transfer from the solid state into an electron-hole plasma.

The material is characterized by its chemical composition and microstructure which determine the type of elementary excitations and the interactions between them. The primary interactions of laser light and matter are always non-thermal. Only optically active excitations can interact with light. In semiconductor materials light can excite free charge carrier and lattice vibrations. The type of elementary excitations strongly depends on the wavelength of laser light. For infrared lasers with photon energy below the band-gap these excitations can be vibrational or excitations created by absorption of light by electrons of conduction band or trapped at the defect levels. The situation changes cardinally when the photon energy of laser light exceeds the gap of a semiconductor material. In this case the light creates electron-hole pairs in material due to interband transitions.

The spatial evolution of incident beam inside the material is described by Lambert-Beer law [14]:

$$I(x) = I_0(1-R) \exp(-\alpha x), \quad (1.1)$$

where $x = 0$ corresponds to the edge of material, I_0 is incident energy; $R = R(\lambda)$ and $\alpha = \alpha(\lambda)$ – reflection and absorption coefficients, respectively.

The light is mostly absorbed at the distance (laser penetration depth) of α^{-1} [15]. The light is mostly absorbed near the surface of target. The photons absorbed in material create electron-hole pairs at the length of α^{-1} . The carrier density can be described by the following rate equation:

$$\frac{\partial N(t, x)}{\partial t} = \alpha \frac{F(x, t)}{h\nu\tau_{pulse}} - k_R N^2(x, t) - k_A N^3(x, t) + \nabla(D(x, t)\nabla N(x, t)), \quad (1.2)$$

where the first term describes the generation of carriers by interband absorption of light with fluence F , photon energy $h\nu$ and pulse duration τ_{pulse} .

The second term corresponds to the radiative recombination of electrons and holes. This process concerns two particles, and this is the reason why the recombination term is proportional to the square of carrier concentration.

The third term of the equation (1.2) describes the Auger recombination. This type of recombination becomes dominant with high concentrations of carriers. Auger recombination involves three particles, and the term is proportional to the cube of carrier concentration.

The last term of the equation (1.2) corresponds to diffusion of carriers in the material. The diffusion coefficient concerns both electrons and holes and can be written in form

$$D = \frac{D_h\sigma_h + D_e\sigma_e}{\sigma_h + \sigma_e}, \quad (1.3)$$

where D_e and D_h stand for the diffusion coefficients of electrons and holes, respectively, and σ_e and σ_h - for the corresponding conductivities.

Equation (1.2) ignores laser induced heating and collective (plasma) phenomena which are important at high carrier densities. In the case of high carrier concentrations optically induced free carrier absorption can produce a measurable contribution to the total absorption:

$$\alpha = \alpha_0 + N\Sigma_{fc}, \quad (1.4)$$

where α_0 is the coefficient corresponding to interband absorption, N – carrier concentration, and Σ_{fc} – effective cross section of absorption by free carriers. The efficiency of light absorption by free carriers decreases rapidly with increase of the laser photon energy $\Sigma_{fc} \sim (1/h\nu)^2$ [14]. For the photons

in infrared spectral region free carrier absorption interband absorption is more efficient than the interband absorption.

1.1.2. Removal of Target Material

The removal of neutral and ionized species from the surface of the targets is a result of transformation (conversion) of energy of elementary excitation to the vibrational energy of atoms. In the case of infrared lasers the photons can be directly absorbed by optical phonons. For UV laser pulses the electronic excitations are more probable. The electron subsystem has negligible thermal capacity and can be heated separately maintaining a low temperature of the rest system. The energy of electronic excitation can be transformed to the vibrations of the localized sites or to the vibrations of the whole lattice with a creation of collective vibrational excitations (phonons).

In the case of a localized process, the electrons of an excited atom pass to antibonding configuration, potential energy of neutral or ionized atom becomes repulsive and this atom can be ejected from the surface during the time needed to perform some anharmonic vibrations. This process is called laser-induced desorption. Desorption is local, nonthermal and can appear even for low laser fluences. The most important for laser induced desorption is photon energy large enough to break the chemical bonds.

Contrarily to desorption, laser ablation is a collective process. Initially, the laser energy is deposited into the electronic subsystem in form of elementary excitations. This energy is transferred to thermal energy of translational and vibrational motion of the atoms in the system and thus increases their temperature. The majority of atoms in the lattice are excited individually or collectively, the chemical bonds are weakened or broken. The temperature rises faster than mechanical relaxation in the system, thus a nearly constant volume heating occurs and the pressure increases. When the pressure gradient in the direction normal to the surface exceeds the mechanical strength of the material, it causes break-up and forwarded ejection of a significant part of the irradiated region, the phase transition appears. The massive ejection of atoms and ions is followed by creation of very dense atomic vapour. Like the others phase transition processes the laser ablation is thermally activated and have a threshold. This threshold results from free evaporation enthalpy of surface needed to break chemical bonds and initiate atom vibrations. The irradiation of material with fluencies below ablation threshold leads to ejection of species by desorption process but does not

lead to formation of vapour with density high enough for effective collisions, thermalization and plasma formation [16].

In most cases material removal is controlled by the rate of thermal conduction through the lattice. The excited electrons transfer their energy to the lattice within a few picoseconds and heating begins within the optical absorption depth of the material $d_{abs} = \alpha^{-1}$. The thermal diffusion length is given by the equation $l_T = \sqrt{2D_T \tau_{pulse}}$, where D_T is the thermal diffusion coefficient. If l_T is smaller than d_{abs} , the bulk will be heated up to d_{abs} . This situation is usual for short laser pulses.

1.1.2.1. Ablation

At the laser fluences used in our experiments, it is assumed that thermal conduction into the solid and consequent thermal evaporation is the predominant ejection mechanism [17]. The equation governing this thermal ejection mechanism is the heat conduction equation:

$$\rho(T)C_p(T)\frac{\partial T}{\partial t} = \frac{\partial}{\partial x}\left(\kappa(T)\frac{\partial T}{\partial x}\right) + (1-R)\alpha I(t)e^{-\alpha x}, \quad (1.5)$$

where ρ is the density of the material, C_p is the heat capacity, T is the temperature, t is the time, x is the depth within the material, κ is the heat conductivity, R is the material reflectivity, α is the absorption coefficient of the material and I is the intensity of the laser irradiation [18]. In the equation (1.5), the absorption coefficient is the only wavelength-dependent term. The absorption coefficient for most known materials rises with increasing photon energy. A high photon absorption coefficient associates with ablation of larger amount of material. Laser excitation with longer laser wavelengths leads to higher heat conduction into the bulk of the material, which means a partial loss of the absorbed power as a heat sink by the thermal conductivity.

The model is in a good agreement with experimental data. A melt front penetrates the solid phase, and the vapour pressure of molten material exhibits exponential growth with temperature. The thermal and optical properties change during melting, resulting in significantly lower thermal conductivity and reflectivity. Material ejection from the molten surface can be described in terms of

thermally activated surface vaporization. The rate of the process is governed by the surface temperature T_S :

$$j(T_S) = \frac{\beta p_0}{\sqrt{2\pi A R T_S}} \exp\left(\frac{\Delta H_{lv}(T_S - T_{lv})}{R T_S T_{lv}}\right), \quad (1.6)$$

where β is related to the sticking coefficient for surface atoms with atomic mass A . R is the gas constant and the terms H_{lv} and T_{lv} are, respectively, the enthalpy and temperature of the liquid-vapour phase transition at an ambient pressure of p_0 .

Removal of the target material by laser ablation with picosecond and longer laser pulses can be divided into three regimes: a low fluence regime that is correlated with non-thermal particle ejection, a higher fluence regime where the laser-material interaction is described by a predominantly thermal mechanism and a high fluence limit where the solid reaches its critical temperature and undergoes phase explosion.

Normal vaporization is applicable at essentially any fluence and pulse duration. The target undergoes vaporization from the extreme outer surface of the melted target without bubble formation [17]. The particles evaporation rate from the target surface is governed by the Hertz-Knudsen equation

$$\dot{\varphi} = \eta P_s \sqrt{2\pi m k T}, \quad (1.7)$$

where η is the vaporization coefficient, P_s is the saturated vapour pressure, m is the mass of a particle, k the Boltzmann constant, and T is the target temperature. The velocity of surface recession is given by the flux multiplied by the cube of the mean interatomic distance $\varphi \Lambda^3$. In terms of the material density, $\Lambda^3 = m/\rho$. The normal vaporization rate for different materials has been evaluated to be lower than one atomic monolayer per nanosecond for the target temperatures below the boiling point [18, 19].

Normal boiling mechanism takes place when the liquefied target surface is heated up to temperatures slightly exceeding the boiling temperature [17, 19]. The vapour bubbles are formed by

heterogeneous nucleation at the outer surface of the liquid, on impurities or defects in the liquid bulk, or at the underlying or enclosing solid surface. Once formed, the bubbles are diffusing and escaping from the liquid surface. The bubble diffusion rates in the melted materials are lower than 1 nm in 1 ns [19]. Thus, the process of normal boiling is extremely slow and can be achieved only for micro- or millisecond pulses [19].

Phase explosion, or the process of explosive boiling occurs when the laser fluence increases sufficiently, and the target almost reaches the thermodynamic critical temperature at and underneath the surface [17]. The mechanism of material ejection and the total flux ejected changes significantly. Metastable superheated state of the melted material is a consequence of rapid heating of the target to temperatures significantly higher than the boiling temperature. Density fluctuations cause the superheated liquid to undergo a phase transition to a mixture of vapour bubbles and liquid droplets spontaneously. Then the ejecting of a mixture of vapour and droplets leads to the relaxation of the system [19, 20].

1.1.3. Gas and plasma dynamics

The massive ejection of atoms and ions by laser ablation is followed by creation of a very dense atomic vapour. The photo- and thermoelectrons are also ejected from the surface. The plasma is created because of collisions of atoms and electrons in the vapour. In the case of nanosecond pulses, this plasma can also absorb the laser light from incident beam and shield the target. This process is very important for long laser pulses and for IR irradiation. The effectiveness of plasma absorption depends on plasma parameters (density), which result from the laser fluence.

The two main absorption mechanisms in a monoatomic ablation plume are multi-photon ionisation (MPI) and electron-ion inverse Bremsstrahlung (IBE) [13]. The two contributions to IBE, electron-neutral and electron-ion, are important during different stages of the heating process. Electron-neutral IBE is considered to play a minor role under these experimental conditions, as for the laser fluences above the plume threshold, ion density increases rapidly [18, 21]. The absorption coefficient for electron-ion IBE varies as the square of the electron concentration, which, in order, increases exponentially with the temperature until the ionization is complete. At the completely ionized stage, the electron density is proportional to the pressure. At this point, the absorption coefficient varies as the square of the pressure.

Both of the absorption mechanisms are wavelength dependent. The probability of IBE scales with the wavelength, while MPI scales with the inverse of the wavelength. Thus the importance of IBE increases at longer wavelengths while that of MPI declines. At the wavelength (1064 nm) used in the experiments, IBE is the dominant mechanism in formation of ablation plasma. MPI, however, might also serve as a seeding mechanism for IBE. The inverse Bremsstrahlung is highly dependent on the ion (and thus the electron) concentration in the plasma, so it is important also during the short-wavelength ablation process.

Mentioned absorption processes in the plume not only heat up the plume, but also increase the ionisation fraction and the electron density, thus forming increasingly denser plasma. At high fluences, the electron velocity distribution that develops from laser plasma heating is no longer described by local thermodynamic equilibrium (LTE) concepts. In this case, charge separation occurs, and, as a result, the positive ions in the plasma are strongly accelerated. The physical mechanisms leading to creation of fast electrons and ions include resonant absorption of the laser photons. In the case of pico/femtosecond laser ablation, the laser-plume interaction is non-existent, since most of the plume development occurs after the expiration of the laser pulse.

Another approach to describe the plume dynamics follows from theoretical hydrodynamical modelling of the rapid surface vaporisation process associated with the laser ablation process.

The particles ejected from the target form a cloud near the target surface. These particles collide and thermalize in this layer, called Knudsen layer (KL). It is a region where the translation equilibrium is achieved by collisions between particles. The thickness of the KL is about five mean free paths. Due to thermalization, the particles in KL obtain the Maxwell velocity distribution in the centre of mass coordinate system. The distribution is described by [22]:

$$f(v) \sim v^3 \exp\left(\frac{m(v-u_0)^2}{2kT}\right), \quad (1.8)$$

where u_0 – velocity of the centre of mass, T – thermodynamical temperature of particles in the system of centre of mass.

When the particles leave KL, the further expansion is described by hydrodynamics. An adiabatic expansion of plasma occurs and the temperatures can be related to the dimensions of the plasma. The density and pressure of the ablated material are decreasing in the direction from the target surface. Initially, in direction perpendicular to the target surface particles propagate faster than in lateral direction, which explains a cigar-like shape of the plume [23]. The thermal energy converts to the kinetic energy, and the plasma expands rapidly with supersonic speed. The temperature drops quickly in the early stages of expansion, but at later time energy is regained in the recombination of ions [24].

In vacuum, the angular distribution of the ejected material is determined mostly by collisions of the plume particles between themselves in the KL and is usually described as following [25]:

$$Y = Y_0 \cos^p(\theta) \quad (1.9)$$

where θ is the angle relatively to the target surface normal. Depending on the laser pulse fluence and wavelength, the exponent p varies between 3 and 50 [25]. In case of the plume propagation in an ambient gas, additional collisions of the plume particles with the gas molecules perturb the angular distribution. During the initial stages, the expansion of plume in gas is similar to the expansion in vacuum. After that, the particles of the plume collide and mix up with ambient gas molecules. The resulting plume broadening becomes important when the pressure of particles in the plume becomes comparable with the pressures of ambient gases. The plume loses the directivity and slows down. At low ambient gas pressures the plume angular distribution can be described by cosine-power law (1.9) with smaller p values [25].

1.2. Plasma facing materials. Plasma-wall interaction

In a fusion reactor, there are components in direct contact with the plasma. The largest surface consists of the first wall which surrounds the bulk region of the plasma torus. The plasma shape may be restricted by additional limiters to protect the vessel wall or equipment like antennas for radio-frequency heating which cannot withstand excessive heat loads. Finally, a very important part of the plasma facing components in current and future fusion devices are the divertor target plates. Divertor is a separate region in vacuum vessel to which escaping ions are exhausted along the magnetic field lines by means of auxiliary magnetic coils. In a diverted plasma configuration these plates provide the main plasma-surface interaction zone. The fraction of the fusion power carried by the produced α -particles is coupled out to a large extent through these areas.

There are two types of plasma configurations: a limiter type and a divertor type. In a divertor configuration the distance of the plasma wetted surface areas to the confined plasma region is much larger than for limiter configurations. Due to the correspondingly lower penetration probability of eroded material, it is much easier to maintain a low impurity level in diverted plasma discharges [26].

In magnetically confined plasma, the plasma is held within closed magnetic flux surfaces generated by a combination of fields due to external conductors and to currents flowing in the plasma. Such fields can only be generated within a restricted volume. Therefore, there is a boundary determined by the last closed flux surface. In case of magnetically confined plasma, the closed surface is determined entirely by the magnetic fields, so that when the plasma ions and electrons diffuse across the closed flux surface, they flow predominantly along the magnetic field until they reach a solid surface [27]. This is the basic geometry of a divertor (Fig.1.1). The region outside the last closed flux surface is referred to as the scrape-off layer (SOL), see Fig.1.2. The particle exhaust and the α -particle fraction of the produced power (as well as the additional heating power during start-up) are coupled out to a large extent through this region and transferred to the limiters or divertor plates.

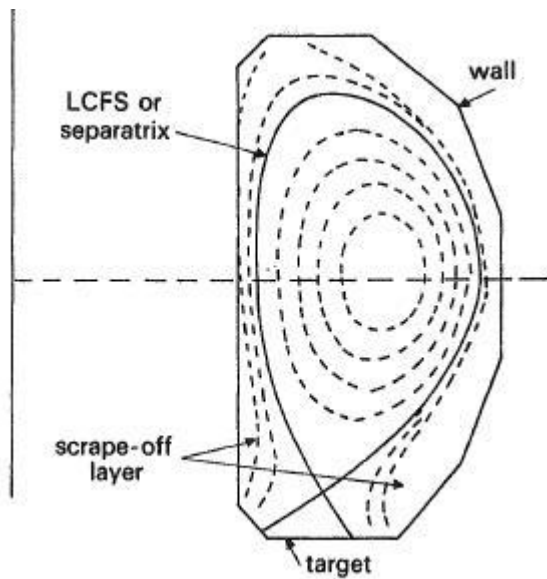


Fig.1.1. Schematic diagram of flux surfaces in a tokamak with a divertor [27]

When wall components are in direct contact with plasma, electrons and ions hit the surface. This particle bombardment is followed by the release of atoms due to collisions and, for certain materials due to chemical reactions. In addition, the wall material is heated by the corresponding energy transfer. Finally, electron impact may produce secondary electrons which are re-emitted back into the plasma.

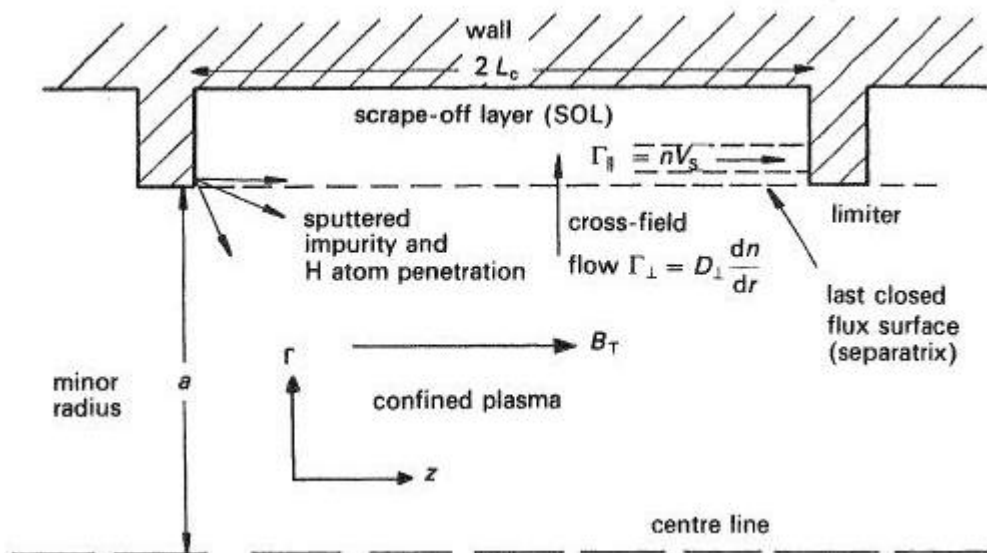


Fig. 1.2. A two-dimensional schematic diagram of the plasma flow from the core plasma into the SOL by cross-field diffusion and parallel flow in the SOL to limiters [27]

Some incident plasma ions are neutralized by the process of reflection, while the remaining part is implanted and may be released with some delay. Neutralized particles entering the plasma are re-

ionized by electron impact or by charge exchange processes with plasma ions. Charge exchange processes in hot plasma regions produce high energetic neutral particles. These particles can escape the plasma even without direct contact with plasma, just hitting plasma facing components. Some of these high energetic particles might hit the walls again and might be re-emitted with some probability.

In fusion devices, plasma facing components are also subjected to intense irradiation by neutrons. This leads to modifications of the material structure and to corresponding degradation of mechanical stability and thermal conductivity.

Wall atoms eroded by the particle bombardment and, in case of excessive heat loads, by evaporation processes, enter the plasma as impurities with harmful effects on plasma discharge. The erosion of wall surfaces limits the lifetime of the respective components. The eroded material, however, migrates through the plasma until it is finally redeposited, which may balance the erosion to a certain extent.

1.2.1. Hydrogen fuel cycle

The hydrogen isotopes used as fuel for nuclear fusion interact with most of the relevant reactor materials. This is important in particular because of:

- radiological reasons: the storage of tritium in the first wall is responsible for the major fraction of the tritium inventory in fusion reactors;
- engineering aspects: hydrogen in solids may alter their mechanical properties in an unfortunate way;
- density control of the plasma: the hydrogen inventory in the walls during a stationary discharge will be much higher than the hydrogen content of the plasma itself, leading to possible difficulties in maintaining a stable plasma density.

At low plasma temperatures, neutral atoms and ions hitting the wall will usually be reflected after transferring a part of their kinetic energy to the material [26].

For high plasma temperatures, the particles can penetrate the material deeply. Then the recycling of the particles will be determined by kinetic reflection, but in addition, the particles may be implanted and reemitted after diffusion back to the surface.

1.2.1.1. Reflection

Ions and neutral particles hitting the wall material will not be reflected right at the solid surface. Usually they will penetrate the material and be scattered by the atoms and electrons in the crystal lattice. Collisions with nuclei will lead to energy transfer and deflection while collisions with electrons will only lead to energy loss. If the path of the penetrating particles leads them back to the surface, they will be reemitted. The particle reflection coefficient R_n is defined by [26]

$$R_n = \frac{\textit{number of reflected particles}}{\textit{number of incident particles}}, \quad (1.10)$$

and can be determined by the computer simulations, as the experiments are very difficult at required energies due to strongly decreasing sensitivity of detectors.

As the reflection is mainly determined by backscattering processes, it therefore increases with the target atom mass. Increasing energy of the incident particles results in deeper penetration into the bulk material, which leads to the observed decrease of the reflection coefficients towards higher energies.

1.2.1.2. Implantation, diffusion and re-emission

The fraction of implanted hydrogen ions which are not reflected, are slowed down by subsequent scattering. They will eventually be trapped either at grain boundaries or at vacancies in the bulk. When the ions enter the solid surface, they recombine to atoms and the fraction which is not trapped. This fraction may then travel through the material by diffusion. If the atoms reach a surface, they recombine to molecules and may be released by thermal desorption.

Carbon as wall material is quite special. For temperatures 400^0 C like in present fusion experiments with graphite as wall material, there is practically no diffusion. Implanted hydrogen is collected until

a saturation level of 0.4 H/C is reached. If the implantation continues, the additional hydrogen is reemitted immediately. After stopping the implantation, the reemission is expected to be much smaller than for metallic wall. In present fusion experiments, the saturation level is reached after some discharges. This may cause problems in controlling the plasma density. With so-called conditioning discharges using helium, the hydrogen inventory can be decreased if necessary.

In a fusion reactor with wall temperatures above 500°C , diffusion and recombination to H_2 become important also for carbon with similar problems for the tritium handling as for the metals. A further process leading to hydrogen trapping in carbon occurs in devices with divertor plates made of carbon, like in ASDEX Upgrade. Carbon atoms produced by erosion of the plate surfaces may be deposited at other locations where they will collect more hydrogen. This leads to a further increase of the hydrogen inventory in the whole vessel.

1.2.2. Methods of impurity production

There are several possible mechanisms by which impurities might be introduced into plasma. These processes are illustrated in Fig. 1.3 [26].

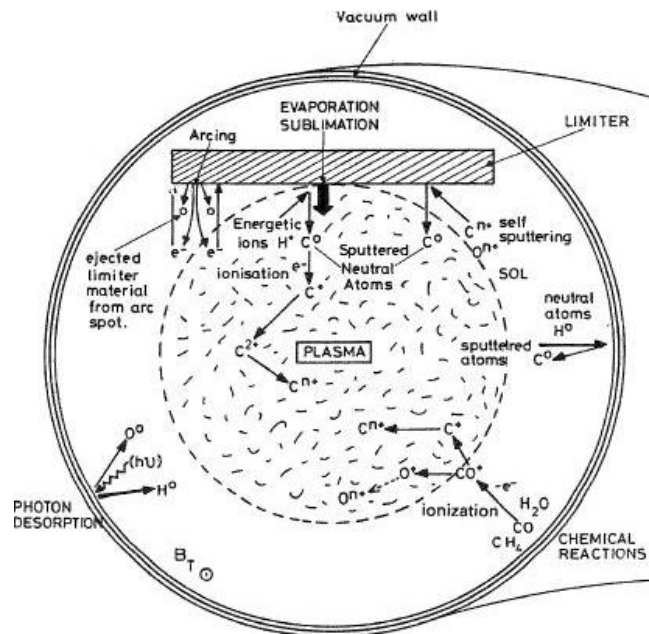


Fig.1.3. Schematic of the various impurity processes occurring at the walls and limiters of tokamak [27]

The bombardment of the wall elements by particles escaping the plasma or streaming along magnetic field lines creates a source of neutral atoms from the wall material. Depending on the location of the surface and the plasma properties in the surrounding area of the source, a certain

fraction of the wall atoms might penetrate the plasma, and get ionized there. The presence of these impurities may degrade severely the plasma properties necessary for nuclear fusion.

1.2.2.1. Sputtering

An energetic incident ion transfers energy to the lattice atoms by momentum transfer, forming a collision cascade. When as a result of such a cascade a surface atom receives sufficient energy to overcome the surface binding energy, it is released from the surface. Therefore, sputtering yields depend inversely on the sublimation energy of the solid and directly on the energy transferred from the incident ion to the lattice atom.

There is a threshold energy of the incident ion below which insufficient energy is transferred to the lattice atom for sputtering to occur. If the incident ion is much lighter than the target atom ($m_2/m_1 > 10$), the threshold energy is given by conservation of momentum [27]:

$$E_{th} = \frac{E_S (m_1 + m_2)^2}{4m_1 m_2} \sim \frac{E_S m_2}{4m_1}, \quad (1.11)$$

where E_S is the surface binding energy of the solid. For most materials E_S is in the range of 3.5 - 9 eV. Therefore, for the same projectile mass, the threshold energy is mainly determined by the mass of the target atoms. In the case of self-sputtering (when $m_1 = m_2$) the collisional cascades are much larger, and the mentioned model is not valid any more. It is described as $E_{th} = 4E_S$.

The sputter yield increases with the angle of incidence of the ion from normal. This dependence is especially important for the high energetic ions. The evaluation of energy distribution of the ions is complicated in the most plasma physics devices. This leads to the difficulties in estimation of sputter yield.

The sputtered wall particles are practically all neutral. Except for single crystal targets their angular distribution is given approximately by a cosine distribution. Their energy distribution has typically a maximum at $0.5E_S \approx 2-3$ eV [26]. Therefore, they can deeply penetrate the plasma before they become ionized which gives them a high probability to become confined in the plasma.

1.2.2.2. Desorption

The surfaces inside the vessel may also be covered with thin layers of water or cleaning agents. Surface impurities result from bulk impurities such as carbon, nitrogen and oxygen in solution in the metal, and also from oxidation, gas adsorption and other contamination of the surfaces because of manufacturing processes. So, there are a large number of impurities in the bulk material. As the surface layer is depleted, a concentration gradient is produced allowing more material to diffuse to the surface.

Processes which are likely to contribute to desorption are thermal, electronic and momentum transfer. Thermal desorption of adsorbed gases is well studied, and desorption rates in dependence of temperature are known. However, data for practical use are irreproducible because of variation of the conditions of the surfaces.

Electron stimulated desorption results from excitation of an adsorbed molecule into a repulsive state which is then repelled from the surface. Energies of the desorbed species are of the order of a few eV. They may leave either as neutrals or ions.

The desorption of surface impurities by ions and neutrals is predominantly a momentum transfer process similar to sputtering. The desorbed atoms would be expected to have energy of several eV. Yields in this case are generally dependent on surface concentration of the impurity.

It is possible to remove the weakly bound layers by glow discharges, however, the remaining oxide layers and adsorbed water molecules cannot be removed and are the main source for the oxygen contamination of the plasma.

1.2.2.3. Evaporation and sublimation

Evaporation can only occur if the surface temperature during the pulse rises close to the melting point. The evaporation rate is directly related to the vapour pressure of the material and the surface temperature. The surface temperature can be obtained from the power flux to the surface, which, in turn, can be estimated from the plasma parameters. Therefore, the possibility of evaporation to occur can be estimated for given pulse length [27].

Laboratory experiments show that in carbon exposed to high level of particle influx, interstitial atoms are produced. They can reach the surface by diffusion where they sublime. This process starts at much lower surface temperatures ($> 800^{\circ}\text{C}$), and could lead to increased carbon production in a fusion reactor [26].

1.2.2.4. Arching and melting

Arching can occur between two electrodes in a vacuum if an external potential is applied. Material is evaporated from the cathode and is ionized, allowing current to flow. The presence of a plasma can lead to an “unipolar” arc where the applied potential is produced by the plasma sheath. Arcs can be detected by examination of the surfaces as they leave characteristic tracks, and these tracks can be observed in the components of fusion devices. However, such arcs and the consequent production of impurities seem only to occur during the initial plasma production or during instabilities. There is no evidence that arching could be a serious impurity generating process under the stable operation conditions in fusion devices. In tokamaks, plasma diffused across the magnetic field lines. Under these conditions, wall tends to charge positively with respect to the plasma. That is why electron emission from solid is suppressed, and the unipolar arc cannot be sustained [27].

If metals are used as wall material, the surface can be destroyed by melting, if the heat load from the plasma becomes so high that it cannot be removed by conduction and cooling. Droplets of molten metal from the upper vessel regions can fall into the plasma resulting in the sudden rise of the radiation losses which, in turn, may cause a break down of the discharge [26].

1.2.2.5. Chemical reactions

Unlike physical sputtering, the yields for chemical reactions are very much dependent on surface temperature. Such yields are sensitive to surface conditions. Yields measured in tokamak conditions are much lower than these in the laboratory conditions. This can be explained by the presence of metals on the graphite surface which may inhibit the chemical reaction rates [27].

1.2.3. Minimizing impurities

1.2.3.1. Vessel conditioning

The first step for minimizing the impurities is to remove the loosely bound impurities adsorbed on surfaces. The most effective techniques for this are baking (thermally desorbs the most weakly bound impurities) and glow discharge cleaning (removes the most of the rest).

For glow discharge cleaning, a positively biased electrode is inserted, and the vessel used as a cathode. Ions and electrons bombard the most of the surfaces of walls uniformly, allowing them to release gases which then are pumped out [28].

Evaporation of reactive metal layers such as titanium, chromium, beryllium, has been effective in reducing problems with adsorbed gases. These materials are particularly good at removing oxygen by adsorption. The process is commonly referred to as gettering [27].

Metallic impurities can only be allowed at very low concentrations. The problem of metallic impurities sputtered from the walls has been minimized by putting a thin film of low materials on the walls. The processes are known as carbonization and boronization in dependence the material being used [29].

1.2.3.2. Impurity screening

The impurities released from a surface may get ionized in the SOL and flow back to the surface not entering into the plasma. In this case, plasma would not be affected by them. The impurity screening is difficult to achieve. The divertor configuration might be improved for impurity screening, as the sources of impurities can be quite far from separatrix. However, computational models show two-dimensional flow circulation which can reduce the effective screening.

1.2.3.3. Materials selection

The impurities with low Z are relatively more tolerable than these with high Z . However, if the effective yield is high, even low Z impurities can be damaging. A figure of merit has been proposed as follows [27]:

$$R = \frac{C}{Y_D(1 - Y_m)}, \quad (1.12)$$

where C is the maximum tolerable impurity concentration, and Y_D and Y_m are the hydrogen and self-sputter yields, respectively.

For very low plasma temperature the ion energy is below the sputter threshold, and R increases. At very high temperatures the sputter yield decreases, and so R increases again. The high mass refractory metals are good at low plasma temperature as their threshold energy for sputtering is high. But even if sputtering can be controlled this way, the power density is a serious problem, especially in large fusion devices. Physical size of the reactor, the fraction of the fusion power with it is possible to radiate, and the magnetic design of the divertor have to be taken into account. This difficulty can be possible overcome by the magnetic sweeping of the separatrix across the target and increasing the radiation in the divertor.

One more important factor concerning the selection of materials is erosion of surfaces. The question is too difficult because of the lack of full understanding of impurity transport. Net erosion will eventually cause rupture of coolant channels, but net deposition will reduce the heat transfer rate.

2. Review of the literature

2.1. Laser-induced ablation spectroscopy

A variety of models for laser ablation are available, operating in different regimes of wavelength, laser irradiance, pulse length, target material, gas environment, and applied to the various applications as pulsed laser deposition, nanoparticle manufacturing, micromachining, surgery, as well as chemical analysis. A large number of models for laser–solid interaction are based on thermal processes being heating of the solid, followed by melting and evaporation. They describe the laser–solid interaction on a macroscopic scale, that is, by the thermal heat conduction equation [30].

Additionally, few kinds of microscopic models have been developed. They are based on the Boltzmann transport equation for electron transport and for electron–lattice interactions [31], or based on molecular dynamics simulations [32, 33]. Because of the long computation time these models are limited to a short time-scale. A mesoscopic model [34] is a connection between the microscopic and macroscopic phenomena. The advantage of the mesoscopic model is that the time-scale is less limited than in molecular dynamics simulations, and the highly non-equilibrium behaviour can be adequately described. A number of analytical models for laser ablation have also been reported [35].

The study on experimental parameters or physical phenomena that may affect an analysis by the laser-induced ablation spectroscopy was preformed by Castle et al [36]. They investigated spatial and temporal dependence of lead emission in LIBS by using optical filters to observe both atomic and ionic emission. The plasma was observed in two orthogonal directions simultaneously, and images were captured by a CCD. The authors found that the ionic emission was confined to a central portion of the plasma, while atomic emission was distributed evenly throughout the plasma. They suggested that spectral imaging of this kind has the potential to improve LIBS analyses since observation of the entire plasma reduces errors which can be caused by the heterogeneous nature of the plasma.

The question of whether or not thermodynamic equilibrium exists in a laser-induced plasma was addressed Rusak et al [37]. A comparison of rotational, vibrational, and excitation temperatures in plasmas formed by Nd:YAG and excimer lasers on graphite targets. They found that while the excitation and vibration temperatures were similar, the rotational temperatures determined in each

case were almost an order of magnitude lower than either the vibrational or excitational. Moreover, the rotational populations were such that it was impossible to determine a single temperature. The authors assumed that different mechanisms of CN formation may have given rise to this multi-temperature distribution. The vibrational and rotational temperatures were higher for the excimer laser-induced plasmas than for the Nd:YAG (1064 nm) plasmas.

The effect of laser wavelength and atmospheric gas on emission of a laser-induced breakdown plasma on copper was investigated by Lee et al [38]. They found more self-absorption in He compared to Ar, because of increased free atom populations in the outer regions of the plasma. Spectral line widths did not correlate well with atmospheric gas. The authors point out that this result eliminates Doppler broadening as a main cause of broadening in the laser-induced plasma. Excitation temperatures were examined and it was found that plasmas induced by UV wavelengths gave higher excitation temperatures than those induced in the IR. This behaviour was explained by the greater shock wave produced by the UV wavelength.

Kurniawan et al. reported on the generation of the shockwave or secondary plasma by a Nd:YAG laser in pressure of 1 Torr [39]. The authors performed imaging the plasma formation in the proximity of an aluminum block, and observed an increase in emission intensity. This allowed confirming the assumption that the secondary plasma was excited by the shock wave. In the other paper of the same authors, a study of the shock wave produced by an excimer laser has been done [40]. They showed that at the reduced pressure, excimer laser-induced plasma forms two different regions. The primary region is of high background, and the secondary one is excited by the shock wave. The latter region allows spectroscopic achieving of higher S/N ratios.

As for the analysis of alloys by laser-induced ablation spectroscopy, this application that been described by several authors and is almost ready for an industrial setting. St-Onge et al. determined Al, Cu, Fe, Pb, and Sn in Zn based alloys [41] using an infrared Nd:YAG laser at laser energies of 75 and 150mJ. Temperatures and electron densities were roughly the same at these two energies. The authors also determined that local thermodynamic equilibrium (LTE) existed in the plasmas at time delays greater than 3 μ s. This validated their use of a Zn emission line as an internal standard in the subsequent analysis. Calibration curves were generated for the elements to be determined using standard reference materials. Detection limits of 10s of ppm were obtained for all elements except Cu which had a detection limit of 544 ppm.

Barbini et al [42] evaluated laser-induced ablation spectroscopy as a remote technique to determine hazardous elements in soils. The emission light was collected by means of fiber optic. Si, Al, Na, and K were determined in soil standards with detection limits between 10 and 100 ppm with precision of 10 %. They found that unless the sampled soil is homogenized and pressed into a disc, the precision could decrease dramatically.

Another laboratory application which may find its place in the industry is depth profiling analysis. Vadillo et al. have used laser-induced ablation spectroscopy to perform depth-resolved analysis of multi-layered samples [43]. The authors used a Nd:YAG (532 nm) laser. The estimated thickness of a layer removed per pulse was between 150 and 500 nm, depending on sample matrix and laser irradiance. For the mono-layer sample, the LIBS results were compared with glow discharge optical emission spectrometry (GD-OES) analysis. The results show that the GD-OES analysis provided better resolution, and therefore more information about the metal-metal interface.

Yoon et al show that the small sample volume probed by laser-induced ablation spectroscopy, which causes precision problems in heterogeneous samples, can be advantageous in elemental mapping [44]. Using a Nd:YAG laser at 532 nm, they determined Ba, Cu, Fe, Mn, Pb, Si, and Sr in polished sections of rock. The analysis took about 30 min, and produced color maps of the distribution of each element in the section examined. Typical concentrations ranged from 100s of ppm for Pb to 10% for Fe.

As for the industrial applications, Hahn et al. have been investigating discrete particle detection and metal emissions monitoring in waste combustion systems [45]. The laser-induced ablation spectroscopy unit sampled on-line, in situ at a natural-gas-fired, pilot-scale waste processing unit. The excitation source was a Nd:YAG (1064 nm, 300 mJ) laser. Individual shots were analyzed in real time for the presence of a given metal analyte. After each 1000 laser shot series, the metal concentrations were determined based on a laboratory calibration scheme. The authors included a detailed theoretical discussion concerning the statistical sampling problem of ablation spectroscopy which results from the finite probe volume, small duty factor, as well as the concentration and size distribution of the metal species. Monte Carlo simulations were used to provide insight into the determination of LIBS parameters and waste stream conditions.

As laser-induced ablation spectroscopy is a virtually non-destructive technique, one of quite popular application is paint analysis. Anglos et al reports a successful diagnostics of painted artworks by pigment identification [46]. Since different pigments have varied metallic elemental composition, its spectral fingerprint can identify an unknown pigment. This approach allowed authors to determine which parts of an 18th century oil painting had been subjected to restoration. They demonstrated minimum destruction to the painting by producing 40 μm diameter craters with a depth no more than 10 μm per shot.

2.2. Plasma facing materials

The plasma wall interaction and the related processes are investigated using wide range of techniques. A detailed 2-D tritium distribution of the plasma-facing wall of ASDEX Upgrade was presented by Sugiyama et al [47] using by TIPT (Tritium Imaging Plate Technique). Imaging Plate is a 2-D radiation detector with high sensitivity and resolution, utilizing a photostimulable phosphor. Tritium activity is expressed as the photo-stimulated luminescence intensity, which is proportional to the absorbed radiation energy. They showed that tritium intensity is high at the dome baffle tile underneath the X point, at the outer divertor region and in the mid-plane and the lower part of the central column. In contrast, at the inner strike point module tiles little tritium was retained. These observations were similar to those observed in JT-60U, which is D-D device, but different from D-T discharge machines like JET. Moreover, the local retention property showed some information of the plasma-surface interaction such as temperature increase of the PFM, impinging of the ion energy and flux and carbon erosion/deposition. They conclude that the tritium profiling together with the carbon deposition profiling could be a valuable diagnostic for erosion/ deposition and hydrogen retention mechanism.

K. Schmid and J.Roth [48] have studied the erosion of tungsten by carbon ions and the simultaneous bombardment of tungsten with carbon and hydrogen isotopes. For the irradiation of tungsten with pure carbon it was found that carbon diffusion in tungsten and enhanced carbon sputtering due radiation enhanced sublimation hinder the protective carbon layer growth during irradiation of tungsten by carbon. To simulate the experimentally observed temperature dependence of the tungsten samples weight change TRIDYN was coupled to the newly developed diffusion code DIFFUSED and a chemical erosion module YCEHM. This combination was validated by comparing them with spectroscopically measured values from ASDEX Upgrade as well as ion beam

experiments using CH_3^+ . The calculations showed that in contrast to pure carbon bombardment, the simultaneous bombardment of tungsten with carbon and deuterium leads to continuous erosion of tungsten.

U. Fantz et al [49] have proposed the molecular radiation of hydrocarbons as a diagnostic tool for chemically eroded carbon by hydrogen. They have completed the correlation of CH radiation with methane particles by a correlation of C_2 radiation (Swan band) with C_2H_y particles. Experimental investigations in laboratory plasmas showed the sensitivity of the intensity ratio C_2/CH on the particle density ratio C_2H_y/CH_4 . The formation of higher hydrocarbons (C_2H_y) can now be taken into account for the determination of carbon fluxes by the simple technique of relative measurements.

One of the main disadvantages of the carbon as a material for the first wall in a fusion device is a process of hydrogen co-deposition. V. Rohde et al [50] have found flakes and two kinds of layers - containing high and low concentration of deuterium - under the divertor structure of ASDEX Upgrade. First investigations were made on these flakes using SEM and ion beam techniques. They have estimated the total amount of carbon outside the divertor to be 1.5g. This amount was deposited in 3000 seconds of plasma discharges. The growing of carbon layer was first measured using a quartz crystal microbalance sensor.

In DIII-D, Buzhinskij et al [51] use a special sample design using DIMES mechanism, in which the graphite sample was arranged to receive the parallel heat flux on a small surface area exposed to plasma from the outer strike point of a DIII-D discharge. The authors have investigated the sample behaviour during exposure to 12 s of plasma. The coatings deposited on the sample and a collector are composed of pure carbon and can be divided into several bands. These bands have different deposition thickness and structure of the coating. They have found irregularly formed grains, globular structure and amorphous carbon.

A. Kallenbach et al [52] have performed spectroscopic measurements of carbon fluxes in the mainly tungsten-coated ASDEX Upgrade tokamak and analysed data with a particle transport and migration code. The carbon concentration in the core and edge plasma is reduced by about a factor 2 only compared to full carbon plasma facing components in spite of 85% tungsten coverage of the primary plasma facing materials. The code reproduced this experimental fact. This behaviour is explained by

the loss flux to the inner divertor in comparison with the strong main chamber recycling of carbon. The quick recovery of the carbon level in the plasma after a boronisation is explained by carbon influx from the outer divertor.

Spectroscopic measurements and HYDKIN code was applied to analyse different hydrocarbon species in TEXTOR [53]. The underlying database for the methane break-up, used in different erosion/deposition models, has been put to test. The chemical erosion yield related to higher hydrocarbons is determined to be lower in the JET outer divertor than measured in previous experiments. In ASDEX Upgrade and DIII-D first in-situ calibrations of hydrocarbon fluxes in the detached outer divertor are performed.

J. Likonen et al [54] have analysed JET Mk-II Gas Box divertor tiles with various ion beam techniques, secondary ion mass spectrometry and Raman spectroscopy. Inner divertor wall tiles removed in 2001 were covered with a duplex film. The inner layer was very rich in metallic impurities, with Be/C \sim 1 and hydrogen isotopes only present at low concentrations. The outer layer contained higher concentrations of deuterium than normal for plasma facing surfaces in JET (D/C \sim 0.4), and Be/C \sim 0.14. Raman and SIMS analyses show that the deposited films on inner divertor tiles are hydrogenated amorphous carbon with low sp^3 fractions. The deposits have polymeric structure and low density. Both Raman scattering and SIMS indicate that films on inner divertor wall.

The study made by E. Fortuna et al [55] has highlighted some conditions influencing the morphology of co-deposited layers. The co-deposited layers were analyzed using TEM, STEM, XPS and SIMS. The layers were accumulated on the collection probes. It has been shown that fuel may be retained in films containing relatively small amounts of carbon. This could have important consequences when developing techniques for fuel and co-deposit removal in fusion devices because layers enriched with metals are also expected in ITER. Therefore, such films as those identified on the ICRF antenna grill may be useful for developing and testing methods of deposit disintegration and removal for the next step machine where the use of carbon will be reduced.

Impurity production, hydrogen recycling and power deposition on carbon and tungsten limiters in TEXTOR-94 have been investigated by means of spectroscopy by A. Huber et al [56]. Different particle and energy reflection coefficients of hydrogen can explain considerable differences

observed on tungsten and carbon surfaces. They found that the majority of carbon release is formed by the recycled carbon, and only a minute part is due to net erosion from the bulk material. The heat deposition on carbon and tungsten side is substantially different under the same plasma conditions, and is typically 30% larger on the carbon side.

Significant progress has been achieved in the understanding of the performance of metal mirrors foreseen for ITER diagnostics [57]. Mirrors are placed inside the fusion device, and then the modification of the surface – materials sputtered during the plasma discharges and erosion of the surface is analyzed. Despite the promising results, there are still a number of open issues which need to be addressed in the nearest future.

3. Experimental techniques

Scheme of the experimental set-up used in this thesis is represented in Figure 3.1, and consists of a Nd:YAG laser equipped with an optical system in order to steer and focus the laser beam, a vacuum chamber, a pump system and a spectroscopic system.

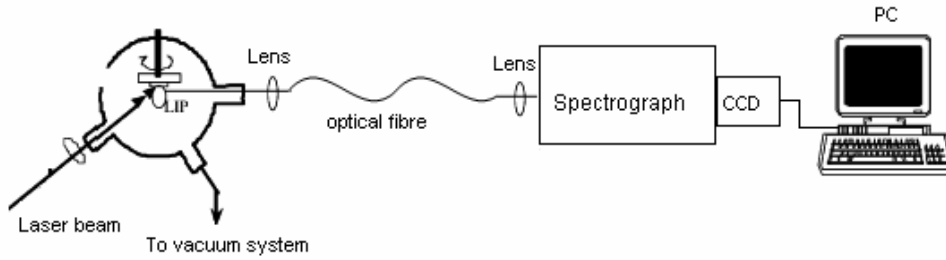


Fig. 3.1. Scheme of the experimental set-up

3.1. Nd:YAG laser

The energy source for material evaporation and atomization in a pulsed laser ablation experiment is a laser. As the experiment requires ablation of possible minimal amount of mass, infrared laser was chosen. It was reported in [13, 15] that the cascade breakdown threshold scales as λ^{-2} , which means that minimal laser intensity required to achieve a breakdown in the metal vapour or in the ambient gas is easier to obtain with an IR laser than with UV. However, the mass ablation rate is larger using an UV laser [58].

For laser ablation, EKSPLA type SL 312 Nd:YAG is used [59]. The parameters for this high peak pumped laser are summarized in the Table 3.1.

Principal wavelength, nm	Maximal pulse energy, mJ	Pulse duration, ps	Focused pulse energy ($\Phi=20\mu\text{m}$), J/cm^2	Repetition rate, Hz
1064	250	150 ± 20	2.5×10^{16}	10

Table 3.1. The parameters of the SL 312 Nd:YAG laser

The scheme of the energy levels of Nd:YAG laser is shown in the figure 3.2 [60].

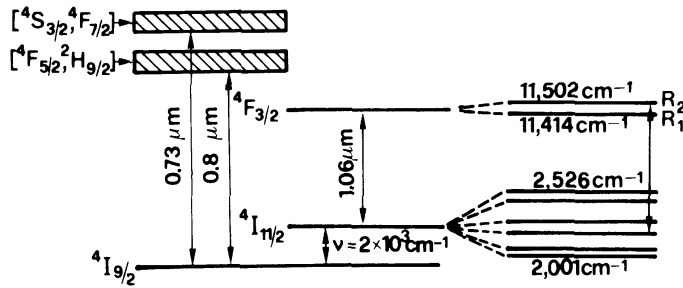


Fig. 3.2. Simplified scheme of Nd:YAG

These levels arise for the three inner-shell $4f$ electrons of the Nd^{3+} ion, which are screened by eight other electrons ($5s^2$ and $5p^6$). Laser action occurs from the upper R_2 sublevel to a particular sublevel of the $4I_{11/2}$ level, as this transition has the highest value for the stimulated emission cross-section. The transition occurs at $\lambda = 1064 \text{ nm}$.

Principal scheme of a master oscillator of SL 312 Nd:YAG laser is shown in Figure 3.3. Oscillator cavity is formed by a mirror (1) and an uncoated glass Fabry-Perot etalon (9) for the longitudinal mode selection. Part of the electro-optical Q-switch (2) between electrodes (a) and (b) is used as classical Q-switch, while another part between the electrodes c) and b) together with the polarizer (3) and PIN photodetector are forming negative feedback.

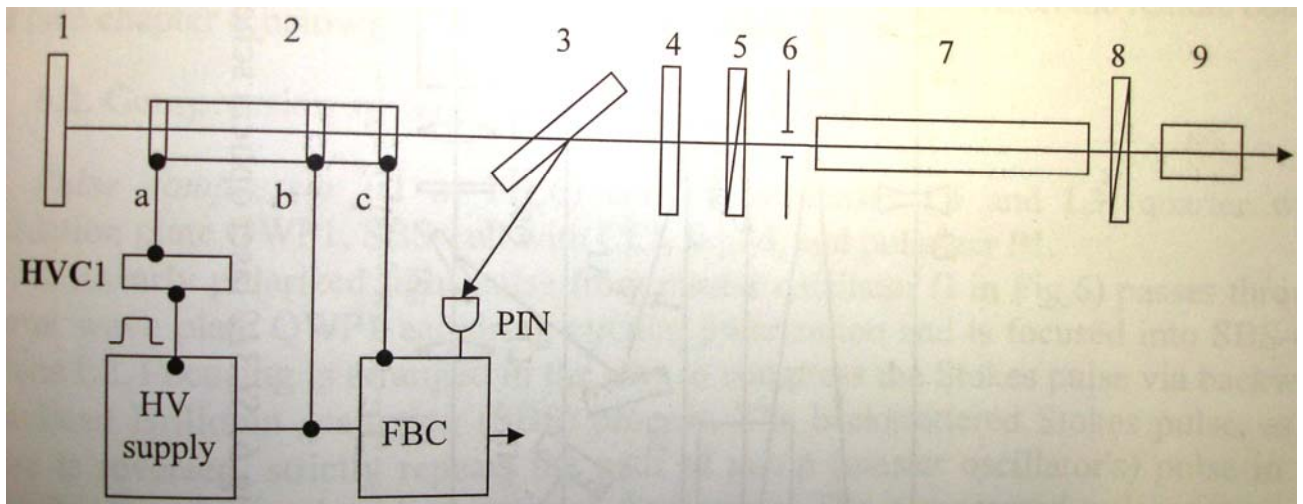


Fig. 3.3. Scheme of master oscillator of SL 312 Nd:YAG laser: 1) 100% reflectivity mirror; 2) electro-optical Q-switch; 3) polarizer; 4) Cr:YAG crystal; 5; 8) quarter wave plate; 6) aperture; 7) Nd:YAG rod; 9) Fabry-Perot etalon; a, b, c) electrodes [61]

The negative feedback is used for selection of single longitudinal mode. At the time when the flash lamp starts to discharge, a high voltage (~3 kV) is applied to the electrode (a) to close the oscillator's cavity when the energy stored in the Nd:YAG rod is below a certain level. Flash lamp continues to discharge, and when the energy stored in active element exceeds the certain level, light begins to escape from the cavity, and free running starts. When lasing appears, a part of light reflected by the polarizer (3) hits PIN photodetector. Voltage generated by the feedback electronics and applied to the electrode is proportional to the light intensity registered by the PIN photodetector. Increased electrode voltage results in light polarization change and the bigger portion of light energy rejected by the polarizer (3). As a result, negative feedback system allows master oscillator keeping lasing at a certain low level for several tens of microseconds. During this time, single longitudinal mode is established due to selective properties of Fabry-Perot etalon (9) and lower gain for the other frequencies. Cr:YAG crystal improves single longitudinal mode selection.

Optimal duration of free running for the establishing of single longitudinal mode is 15-20 μ s. However, the time of the beginning of free running depends on the quality oscillator's cavity and therefore on thermal and mechanical stability of optical components. Autocorrection of closing high voltage adjusts the optimal time for free running to begin. Laser control unit measures the duration from the beginning of free running to the moment of the opening of Q-switch and regulate high voltage to keep the necessary value.

When single longitudinal mode is established, high voltage on the electrode (a) is grounded. Losses of the cavity are decreasing rapidly and Q-switched pulse is emerging from the oscillator.

Oscillator contains an additional aperture (6) for the single transversal mode selection. Quarter wave plates (5) and (8) prevent the interference and hole burning effects in the active element.

Pulse compression is implemented in the following way. A linearly polarized light pulse from master oscillator passes through the quarter wave retardation plate acquiring circular polarization and is focused into SBS-cell. Focusing is arranged in a way to compress the Stokes pulse via backward stimulated Brillouin scattering (SBS) process. The backscattered Stokes pulse repeats the path of the master oscillator's pulse in the opposite direction. The compressed pulse passes the retardation plate that transform polarization of the Stokes radiation into linear and perpendicular to the polarization of

master oscillator radiation. Polarizer rejects the light having vertical polarization and mirrors guide the beam into the amplification stage.

Power amplifier is based on laser chamber containing Nd:YAG rod pumped by a flash lamp and includes optical components arranging three passes through the active element.

The fundamental wavelength of the SL 312 Nd:YAG laser can be frequency doubled, tripled and quadrupled inserting into the beam path the nonlinear crystals generating corresponding harmonics.

The output power of the laser beam was monitored by the power/energy meter (Ophir, model PE25BB-DIF).

3.2. Vacuum chamber

The vacuum chamber for these experiments was constructed and manufactured at the workshops of the Institute of Solid State Physics. The drawing of the chamber is given in the Appendix 1. The vacuum chamber is shown in Figure 3.4. The positioning device inside the chamber allows the sample to be adjusted horizontally. Rotary motion feedthrough provides rotation of the sample, so that various series of experiment can be accomplished at the same conditions. All the viewports are equipped with quartz windows. The entrance port for the ablation beam is designed to be sufficiently longer than the others in order to protect the viewport from contamination with the particles coming from within the plasma plume (ablation is performed normally to the sample surface). Laser beam was delivered to the chamber through the lens of focal distance of 300 mm. During the ablation, some material is unavoidably deposited on the windows, so they are cleaned if necessary.

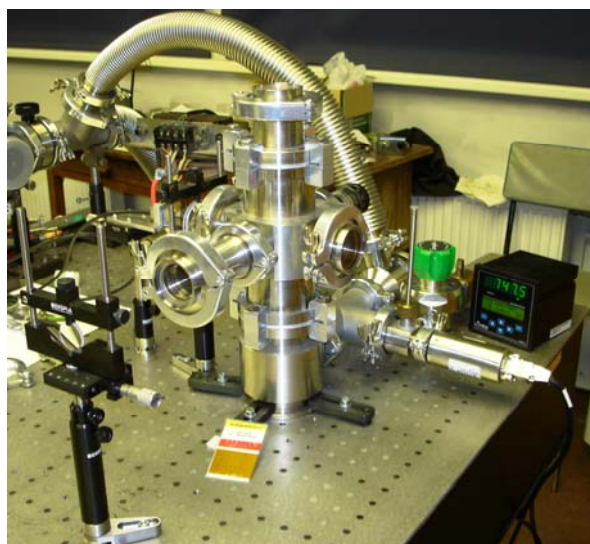
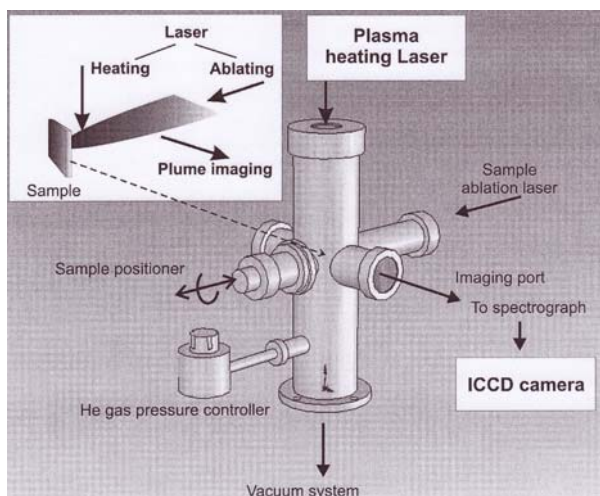


Fig. 3.4. Vacuum chamber used in the experiments

The development of the vacuum chamber allows the easy modification of the system so that a second laser for double-pulse experiment can be attached. The plasma can be heated from the upper viewport.

The chamber is connected to the turbomolecular pump (CDK 280 Ilmvac) providing a vacuum up to 10^{-5} Torr. The pumping system can be isolated from the vacuum chamber via an angle valve. The vacuum system is equipped with a pressure controller 910 DualTrans sensor transducer (MKS Instruments) combining absolute piezo sensor and MicroPirani. The range of the pressure measurable with this assembly is 8×10^{-6} to 1500 Torr. Throughout this work, ablation conditions described as vacuum will refer to a base pressure of $\sim 10^{-5}$ Torr.

A helium delivery system has been developed, so the background gas can be changed.

Outside the imaging port, there is a holder for an optical fibre coupled to the spectrograph and CCD camera. The CCD detector imaging was performed through the side flange. A lens with a focal distance of 50 mm collecting the emitting light is mounted at the distance of 5 cm of the side flange. The light is imaged onto the fibre optics bundle and then transmitted to the slit of an Andor Shamrock sr-303i spectrograph.

3.3. Target Materials

Two kind of the ablation materials were used in this thesis. For the reference measurements, R 6710 graphite was used. The technical information on this material is given in Appendix 2. The samples drilled out of the ASDEX Upgrade (AUG) divertor tiles after they were subjected to plasma discharges is the next material used in this study. Figure 3.5 shows both unablated and ablated samples.

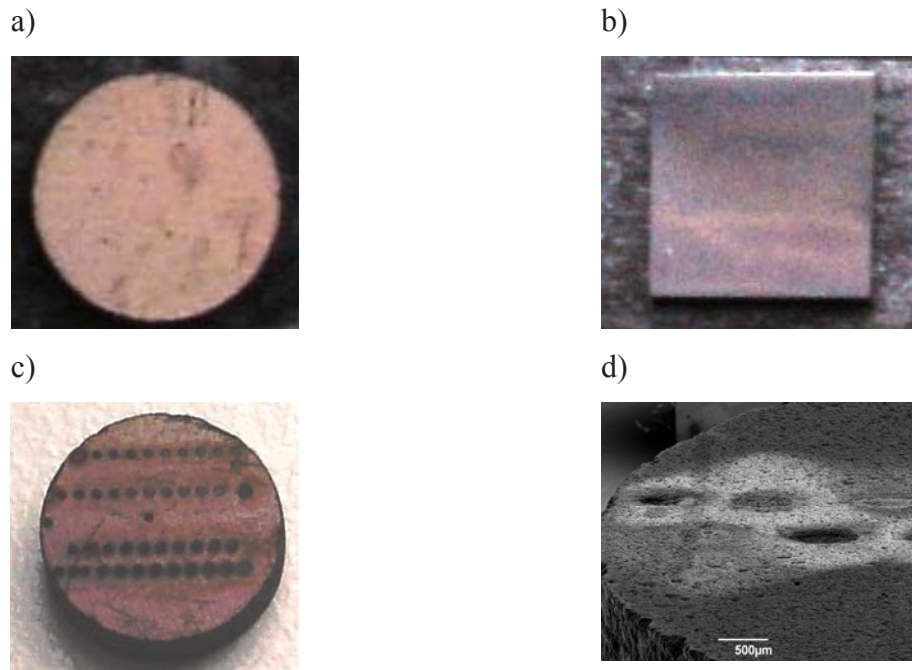
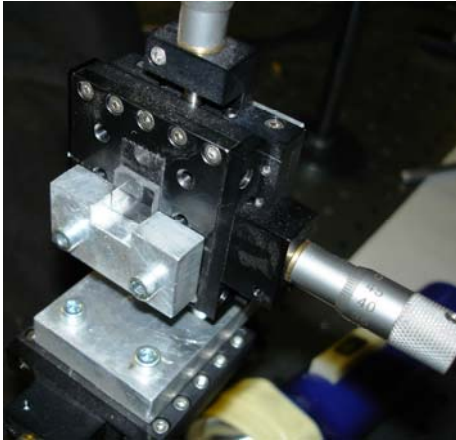


Fig. 3.5. Samples used in this thesis: a) unablated ASDEX Upgrade target; b) unablated graphite R6710 sample; c) ablated ASDEX Upgrade target; d) SEM image of an ablated ASDEX Upgrade target

3.4. Target holders

Two different types of the target holders were used in this study. For ablation in air, a XYZ-translation stage was used (Fig. 3.6 a).

a)



b)

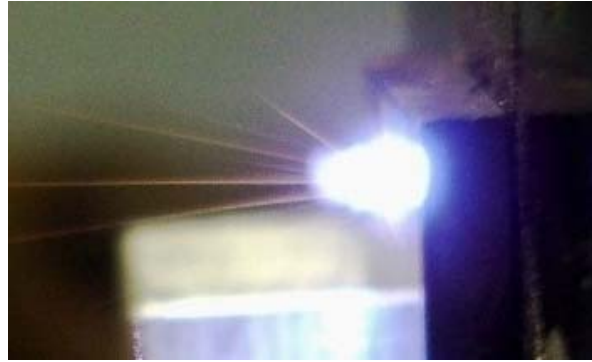


Fig. 3.6 a) A photograph of the XYZ translation stage used for the ablation experiments in air; b) a photograph of laser-induced ablation plasma in air

The first assembly consists of a XYZ target directed at an angle of 90° with the incoming laser beam (fig. 3.6 a). It can be moved manually to a desired direction to provide a fresh space for the ablation. The second assembly for ablation in vacuum consists of a rectangular sample holder mounted to the rotating feedthrough. This holder is inserted into the vacuum chamber. It can be also modified to use round-shaped samples (Fig. 3.7). The shape of the samples is dependent on the RBS target holders (this technique is described further in this chapter).

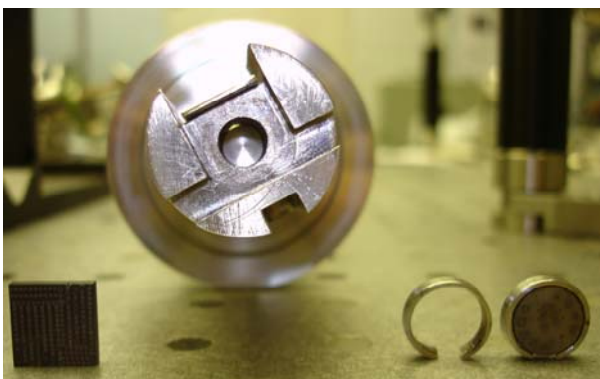


Fig. 3.7. A photograph of the target holders used for the ablation experiments in vacuum. The round-shaped sample can be inserted into the stainless steel detail and placed in the holder

The rotating feedthrough can be rotated manually to provide the intact areas of the sample for the analysis.

3.5. Plasma detection equipment

The laser ablation event produces a time evolving plasma cloud. This plasma can be studied by a number of different techniques. The easiest and most common technique for analyzing the plasma is optical emission spectroscopy. The optical emission arising from the plasma can be viewed using a quartz fibre to couple the emitted light into a spectrograph assembly coupled to the CCD detector. Optical emission from the plasma formed by the incident fluences used in the present work is clearly visible by eye. This emission can be studied with the assembly shown in Figure 3.6 b.

The optical emission arising from the plasma is focused by a lens with a focal distance of 300 mm onto the front end of a quartz fibre optic bundle (Z-Light, Ltd.). The input end of the fibre optic is circular (Fig. 3.7 a). In the output of the fibre, the individual fibres are arranged in rectangular shape to match the entrance slits of the spectrograph.

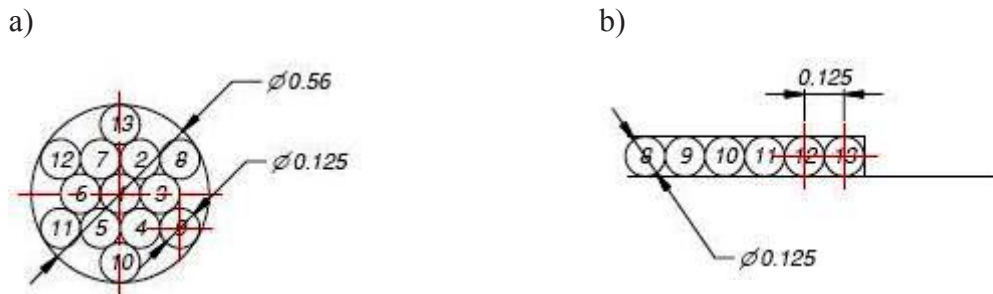


Fig.3.7 a) Input and b) output ends of the optical fibre. All the dimensions are in millimetres

The emission light from the output end of the fibre bundle is collected to the slit of the spectrometer using a quartz lens of focal distance of 50 mm. The spectra are wavelength calibrated by recording the dispersed emission spectrum of the room lights, which contains strong mercury emission lines.

3.6. Rutherford backscattering spectroscopy

The concentrations of deuterium and boron in the samples cut from the divertor plates of ASDEX Upgrade were measured by means of Rutherford backscattering spectroscopy (RBS) at the Max-Planck-Institut für Plasmaphysic, Garching.

The RBS instrumentation comprises the following components: an ion source – alpha particles; a linear particle accelerator, and a detector measuring the energies of backscattered ions. In Garching, two-stage (tandem) accelerator is used. It has a source of He^- ions and a positive terminal at the centre of the accelerator. A stripper element is included in the positive terminal converting He^- ions into He^+ ones. As the ions become positive, they exit the tube at the ground.

The energy loss of the backscattered ion is dependent on the scattering with the sample nuclei. This, in turns, depends on the scattering cross-section of the nucleus and therefore on its mass and atomic number. Nuclei of two different elements will scatter incident ions to different degrees with different energies for a given measurement angle. The output of the measurement is separate peaks on counts versus energy.

3.7. Profilometry

The Dektak 150 profiler takes measurements electromechanically by moving the sample beneath a diamond-tipper stylus. The high-precision stage moves a sample beneath the stylus according to a user-programmed scan length, speed and stylus force. The stylus is mechanically coupled to the core of a linear variable differential transformer (LVDT) [62].

The stage moves the sample, the stylus rides over the sample surface. Surface variations cause the stylus to be translated vertically. Electrical signals corresponding to stylus movement are produced as the core position of the LVDT changes. The LVDT scales as an AC reference signal proportional to the position change, which in turn is conditioned and converted to a digital format through a high precision, integrating, analogue-to-digital converter. The digitized signals from performing a single scan are stored in computer memory [62].

4. Results and discussion

For all experiments, the laser beam was focused at a distance of 3 mm behind the sample surface in order to increase the diameter of the crater relative to its depth, and to avoid spark ignition in air [63, 64]. In case of slight defocusing of the beam, the ablation of the minimal amount of mass can be achieved (fig.4.1).

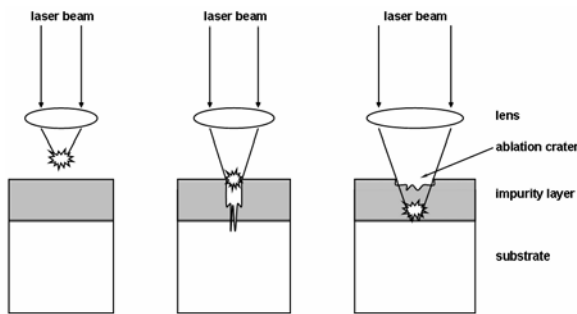


Fig.4.1 Laser beam focusing onto the sample

Placing the target in the focus of the laser beam leads to the formation of excessively deep crater and removal of the most informative layer with the first pulses. Moreover, if the depth of the crater is several hundred nanometres, it is negligible in relation to the diameter, which is several hundred microns; hence a one-dimension evaporation model can be used to describe the ablation process [63].

It is stated that, for example, an average growth of the deposited carbon layer in divertor region is about 0.2 nm/s. Depending on the number of discharges, the thickness of a layer can reach up to 500 nm [65]. The information about the layer growing on the plasma facing materials must be gained approximate within this range of thickness.

4.1. Ablation in air/atmospheric pressure

To investigate the content of the impurities of the ASDEX Upgrade sample taken from the divertor region of the tokamak, laser-induced plasma emission spectra were recorded. An unexposed graphite R7610 sample was used as a reference sample. This sample contains no impurities which are typical for the tokamak sample. To get the profiles of the characteristic spectral lines, 10 laser pulses of energy of 10 mJ were applied on the both samples [66]. The spectra are represented in Fig.4.2.

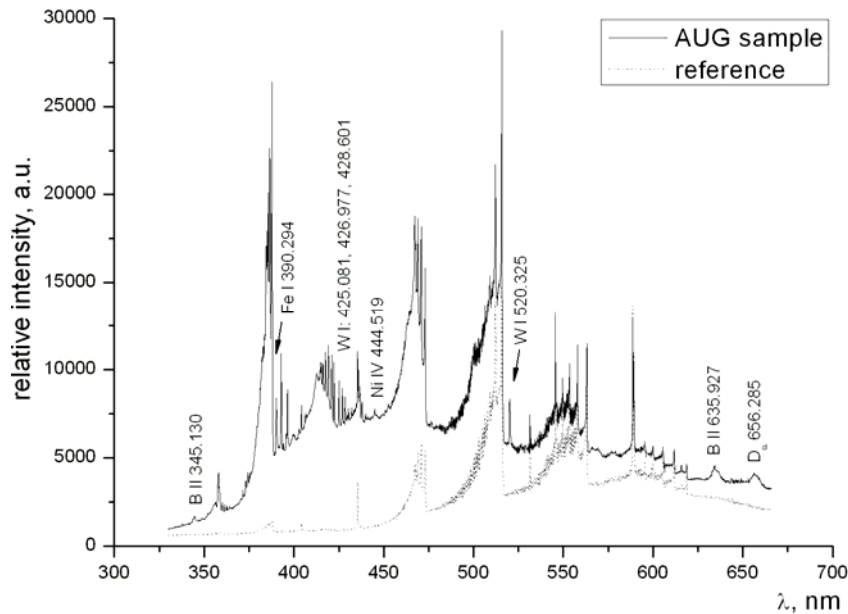


Fig.4.2. Laser-induced plasma emission spectra of graphite R7610 reference and ASDEX Upgrade sample. Carbon lines are not specified on the figure [67]

The spectrum of the ASDEX Upgrade sample shows a substantial number of impurities. Tungsten lines (W I 425.061 nm, 426.977 nm and 428.601 nm) are detected as tungsten is a main material for first wall the coverage in ASDEX Upgrade [68]. The most possible reason for the appearance of B II (345.130 nm, 634.927 nm) lines might be a process of boronization of plasma-facing components - a procedure of surface conditioning [69]. Surface conditioning is made to optimize the influence of the plasma facing components on the plasma performance. An unconditioned wall releases gaseous species, which can prevent stable plasma operation. In order to minimize the gas release, surface conditioning reduces the wall inventory [70].

The source of Fe I 390.294 nm and Ni IV 444.519 nm might be stainless steel components which are not shielded from the plasma, mainly at the outer main chamber wall and additionally the outer covering of electric cables [71]. These cables are moving during discharges, and this movement is the reason of crack formation. Release of material out of these cracks may lead to the formation of dust [72, 73] which migrates through the machine and is afterwards redeposited at various positions.

Although both of the spectra were recorded under the same conditions, the relative intensities of the spectral lines belonging to the reference sample are considerably lower than those of the ASDEX Upgrade sample. This might be due to surface differences in the ablated samples (see figure 3.5 a, b). Reference graphite R7610 sample was polished smoothly in contrast to the

ASDEX Upgrade sample, which is much rougher and demonstrates the traces of erosion after the plasma discharge. Also, the ablation rate differs substantially for these samples. For ASDEX Upgrade sample the average material removal rate was about 0.5 μm per single laser pulse. However, for pure graphite sample this value was close to 70 nm. This is in agreement with the fact that target reflectance determines the amount of laser pulse power absorbed by the material [74]. Additionally, surface defects are of great importance as they contribute to decreasing the laser intensity threshold required to initiate vaporization of the surface [13].

The plasma electron temperature was deduced from the Boltzmann plot method [75 - 77]. If the plasma is assumed to be in the local thermodynamic equilibrium, the Boltzmann distribution can be used to estimate the population of the excited state, and it can be written as

$$n_{nm} = n_n \frac{g_m}{Z} \exp\left(-\frac{E_m}{kT}\right), \quad (3.1)$$

where n_{nm} is the population of the m th excited level, g_m is the statistical weight of the upper level of the transition, E_m is the excitation energy, k is the Boltzmann constant, and T is the temperature. The emission intensity of a line is related to the population of the excited level through

$$I_{nm} \approx A_{nm} n_{nm} \frac{hc}{\lambda_{nm}} = A_{nm} n_n \frac{g_m hc}{Z \lambda_{nm}} \exp\left(-\frac{E_m}{kT}\right), \quad (3.2)$$

where A_{nm} is the transition probability and λ_{nm} is the wavelength of the line. Hence, the temperature can be estimated using the ratio of line intensities. The temperature was estimated using the intensities of several C II lines. A plot of $\ln(I\lambda/Ag)$ versus E for multiple spectral lines should be a straight line of slope $1/kT$. The use of several lines has the advantage of improving the accuracy of the temperature measurement. The designation and other spectroscopic constants used for determining the excitation temperature for carbon are given in the table 4.1. Transition probabilities A_{nm} and the statistical weights g_m of these lines are obtained from the literature [67].

Wavelength λ , nm	Energy (eV), upper level	Statistical weight g_m	Transition probability A_{nm}
512.521	22.6	4	3.21×10^6
515.109	23.1	4	4.16×10^7
564.087	22.9	4	1.97×10^7
589.159	20.1	2	3.49×10^7

Table 4.1. Spectroscopic data of C II lines used for temperature determination [67]

A typical Boltzmann plot used for calculating the excitation temperature is shown in figure 4.3.

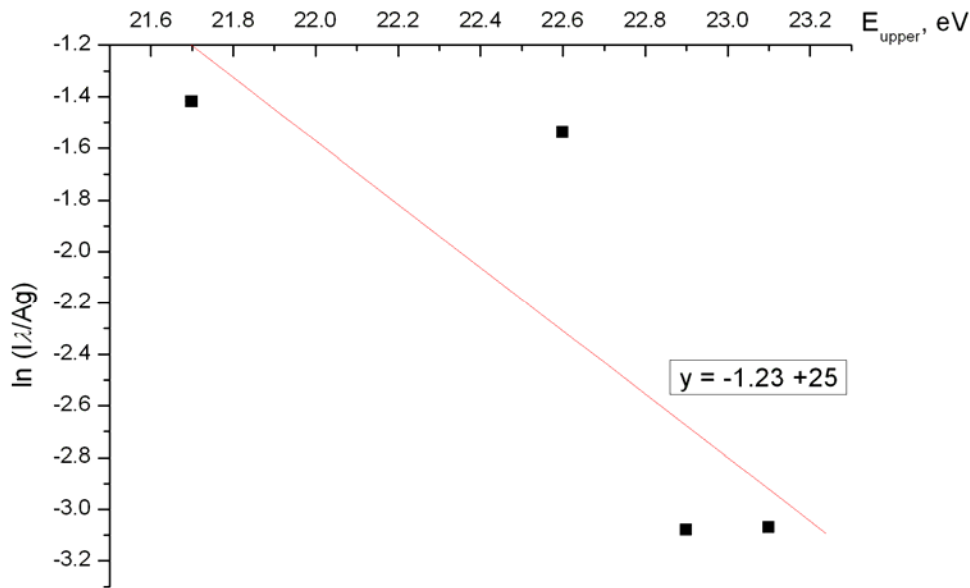


Figure 4.3. Typical Boltzmann plot used for temperature estimation. The intensities of C II lines are used (see fig.4.2). The inverse slope of the best fit gives the temperature. The plot corresponds to laser-induced emission spectrum intensities recorded at the focal spot (laser energy was 10 mJ), which corresponds to a temperature of 0.8 eV.

The main element of interest during the investigation of plasma facing materials is hydrogen and/or its isotopes, in the case of ASDEX Upgrade – deuterium line 656.285 nm. D_α 656.285 nm line has been detected in the investigated sample. To be sure that the detected line is exactly deuterium line, spectra of two samples – ASDEX Upgrade wall sample and graphite R7610 sample which was not exposed to the plasma discharge – were taken in a narrow spectral window of 620 to 680 nm. The related spectra are represented in figure 4.4. The spectra of unexposed graphite R7610 sample does not exhibit neither B II (634.927 nm) nor D_α (656.285 nm) line, which means that these impurities are specific exactly for the samples exposed to plasma discharges.

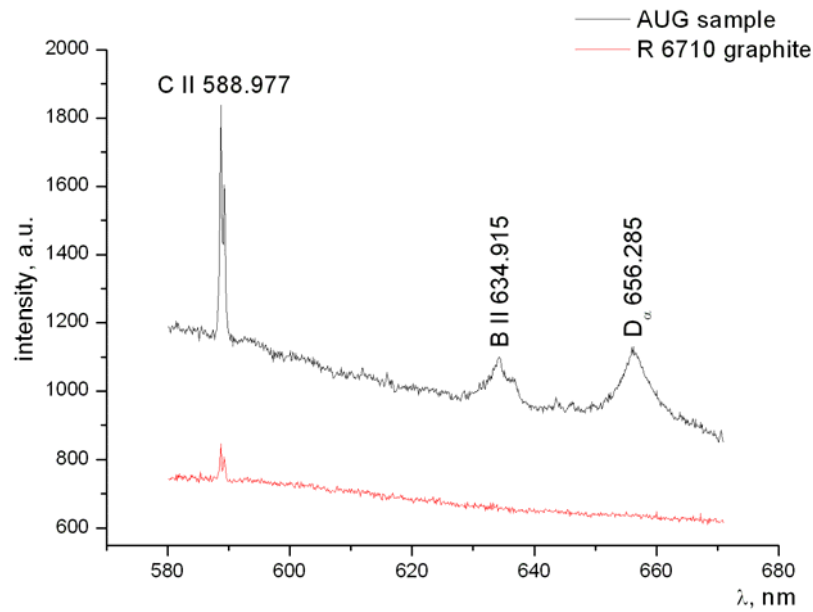


Fig.4.4. Comparison spectra of AUG sample and graphite R6710 sample. One pulse at energy of 10 mJ was accumulated. D_{α} 656.285 nm line was not detected in unexposed sample

To follow the evolution of the appearance of deuterium 656.285 nm line in the spectrum, signals in the spectral window of 580-680 nm were recorded. Fig.4.5 represents spectra corresponding to the 1st, the 2nd, the 3rd, the 5th and the 10th consecutive laser pulses applied at the same spot of the sample.

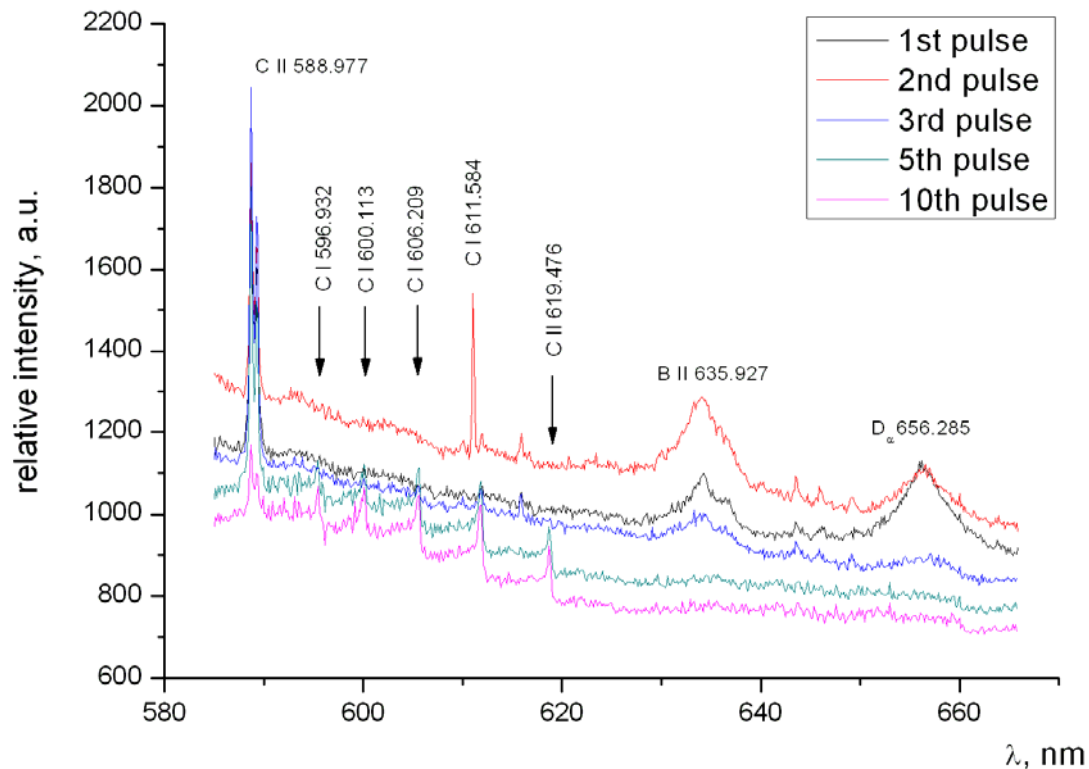


Fig.4.5. Appearance of D_{α} 656.285 nm line [66] in the laser ablation spectrum of ASDEX Upgrade sample. The numbers in the legend correspond to the number of the pulse in the sequence

D_{α} line appears after the 1st laser pulse. Afterwards, the decrease of deuterium signal in comparison with the carbon line is observed. D_{α} line has nearly vanished after applying the 2nd laser pulse. Figure 4.6 demonstrates that by the end of the series of laser treatment the intensity of D_{α} line has decreased almost two-fold compared to that after the 1st pulse. After a sharp decreasing of the intensity of deuterium line, the signal becomes practically equal to the background level.

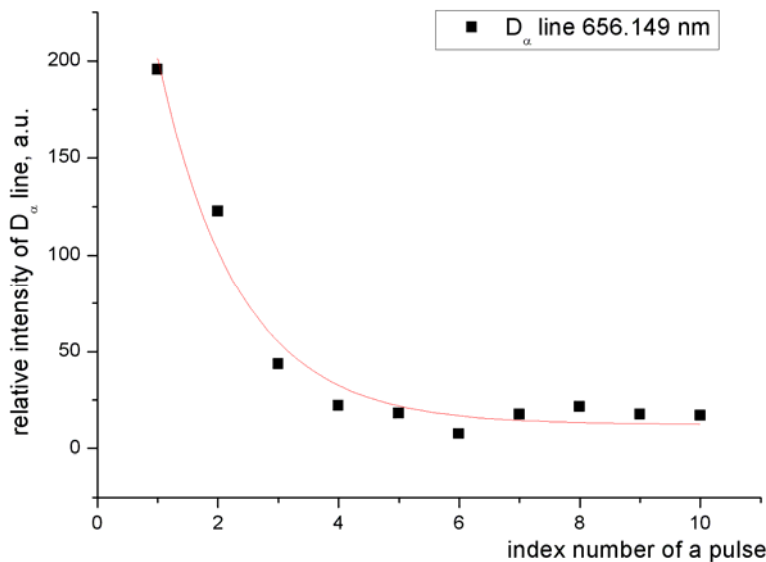


Fig.4.6. Depth profile of D_{α} 656.285 nm line [67] in the laser ablation spectrum of ASDEX Upgrade sample. The average material removal rate was about 0.5 μm per a laser pulse

The behaviour of the intensity of B II 634.915 nm line is depicted in figure 3.7. In contrast to the intensity of deuterium line, the maximum has been reached in with applying the second laser pulse to the AUG target. With the fourth pulse, the intensity of the B II 634.915 nm line has decreased 8 times in comparison to the second pulse, and after the fourth pulse is practically equal to the background level.

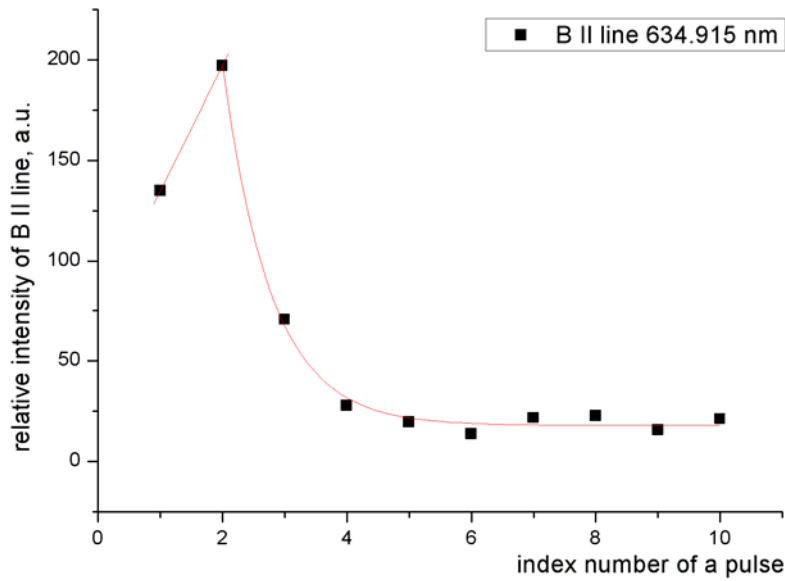


Fig.4.7. Depth profile of B II 634.915 nm line [66] in the laser ablation spectrum of ASDEX Upgrade sample. The average material removal rate was about 0.5 μm per a laser pulse

Figure 4.5 shows that the spectra of C I-II become richer in lines with the number of applied pulses. However, the behaviour of the line intensities resembles the one of deuterium and boron (figure 4.8). The increasing of intensity is followed by decreasing after the fourth applied laser pulse, but the intensity is not decreasing sharply to the background values. After the 8th pulse the signal should remain consistent as carbon is the basic material of these ASDEX Upgrade samples.

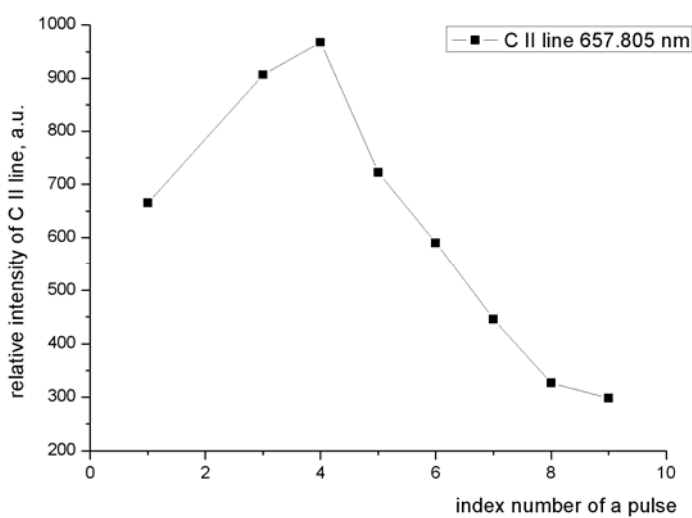


Fig.4.8. Depth profile of C II 657.805 nm line [67] in the laser ablation spectrum of ASDEX Upgrade sample. The average material removal rate was about 0.5 μm per a laser pulse

Figures 4.6-4.8. demonstrate the spectra obtained after ablation of the AUG sample № VI. The concentration of deuterium measured by RBS is 5.36×10^{17} atoms/cm³, the concentration of boron - 9.78×10^{18} atoms/cm³. If the ablation removal rate is about 0.5 μm per laser pulse, deuterium can be situated in a depth of 0.5 – 1 μm inside the bulk material. The concentration of boron, on the other side, reaches its maximum on about 1 μm in the surface, and then the concentration decreases.

The mechanism of laser ablation of the divertor material of ASDEX Upgrade tokamak may be described as follows. When the laser pulse interacts with the target surface, the elements of the impurities appear in the spectrum. This happens as the impurity layer on the ASDEX Upgrade target is removed by the ablation process. The layer could be as thick as $(3 \div 4) \times$ material removal rate, which is around 0.5 μm per laser pulse (fig.4.9).

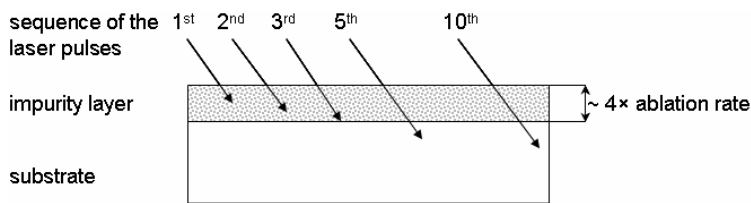


Fig.4.9 Process of the ablation of impurities in ASDEX Upgrade target

The relative intensities of spectral lines corresponding to the impurities and carbon change drastically when the number of laser pulses applied to the same spot increases. The signal of the impurities decreases from high values to the background level. The signal of the substrate of the ASDEX Upgrade target remains consistent with the growing number of applied pulses. The first pulses show only the most intense CII 588.977 nm line, while the other C I-II lines start to appear after the end of the 5th pulse.

These observations are in agreement with the models and experimental results of laser-induced plasma plume propagation. In atmospheric pressure, the plasma is constrained to small volumes close to the target surface. As the forces sustaining the high pressure region of the plume dissipate, the propagation decelerates and the front edge relaxes. This leads to a portion of plume material being deposited back on the target surface. More volatile elements will condense out of the cooling plasma later than more refractory phases. This condensed material presents a source of the refractory element enriched material which is sampled at the later stages of ablation [78].

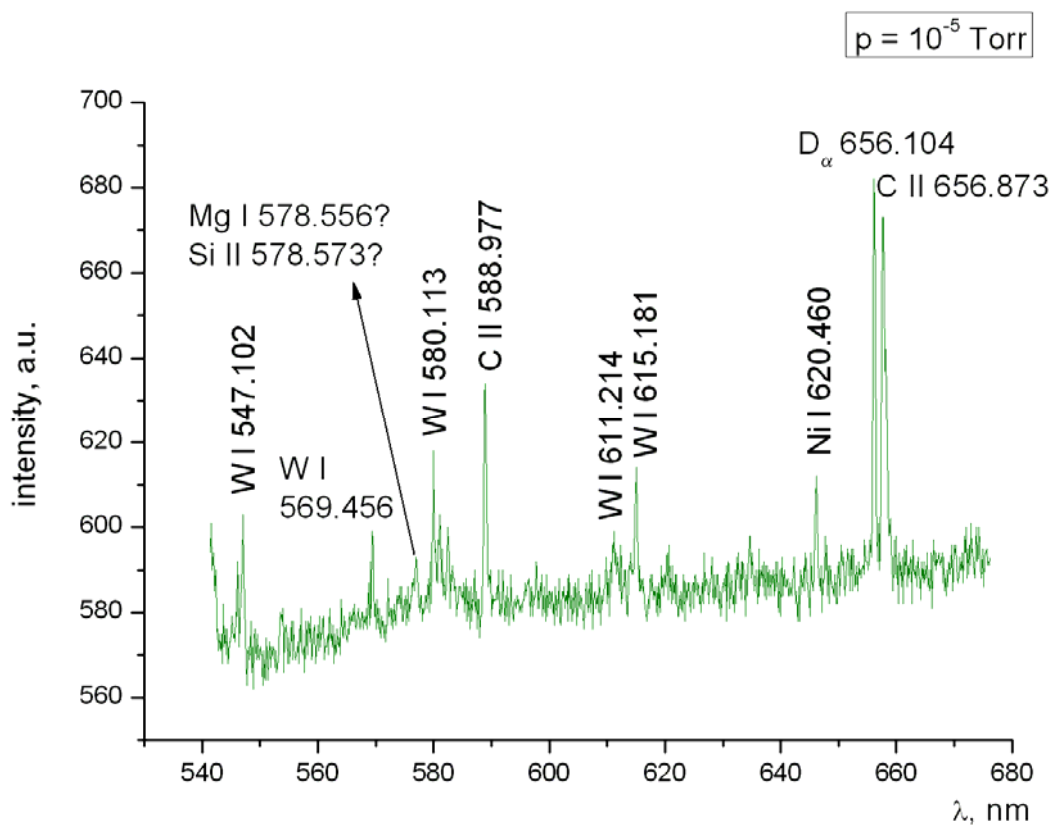
4.2. Ablation in vacuum

The plume characteristics were analyzed by laser-induced spectroscopy. The plume originated from the ablation spot and viewed perpendicularly to the plume propagation direction. The plume parameters are dependent on the laser fluence, and the observed optical emission varies with distance from the target surface.

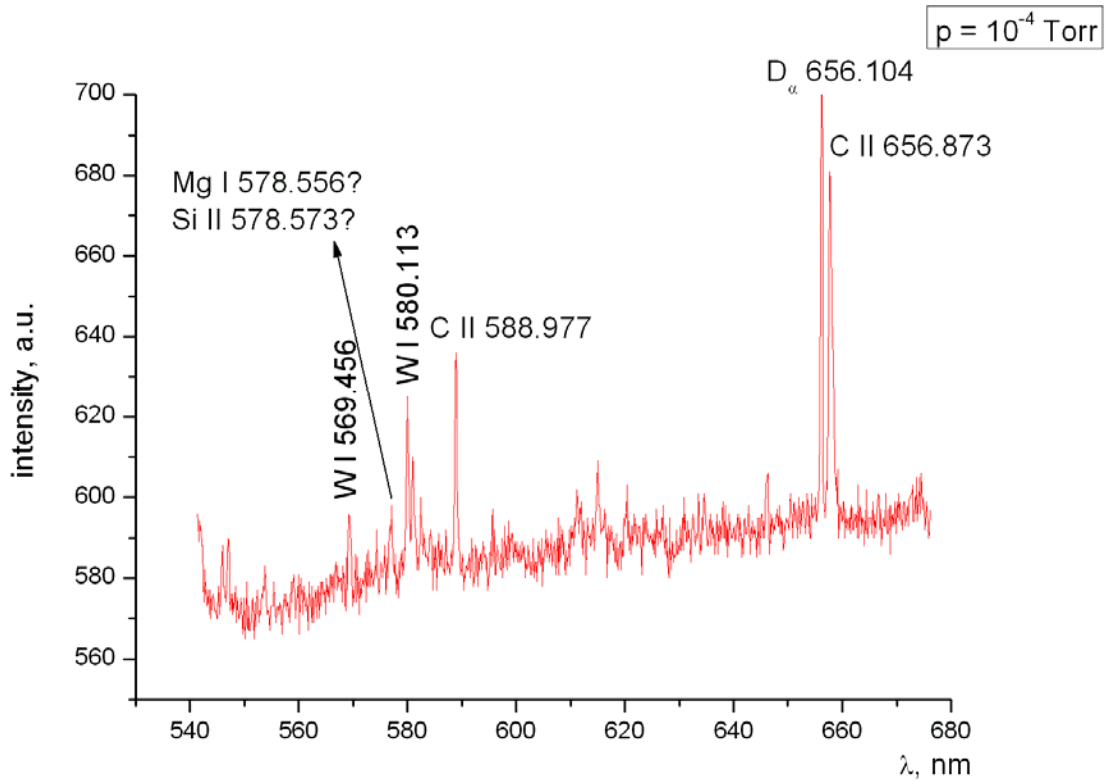
4.2.1. Ablation at different pressure values

In order to find the optimal regime for the depth profiling of the plasma facing materials, the experiments were carried out at three different pressures in a vacuum chamber, and at the atmospheric pressure. A sequence of 10 laser pulses of $\lambda=1064$ nm at the pulse energy of 25 mJ were applied on the targets. Obtained spectra are demonstrated in Fig.4.10. The legend on each series of laser-induced ablation spectra indicates the pressure value. For each pressure, 10 spectra were recorded, and 3 spectra were registered at the atmospheric pressure [79].

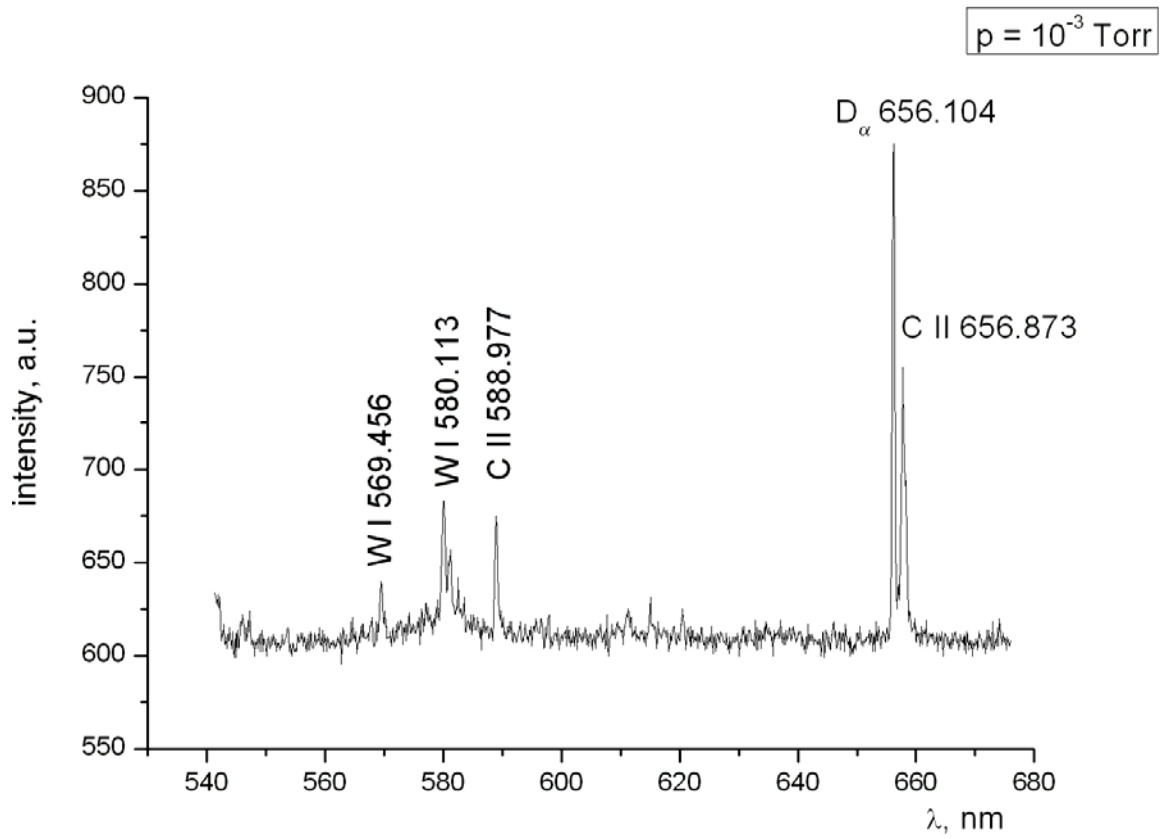
a)



b)



c)



d)

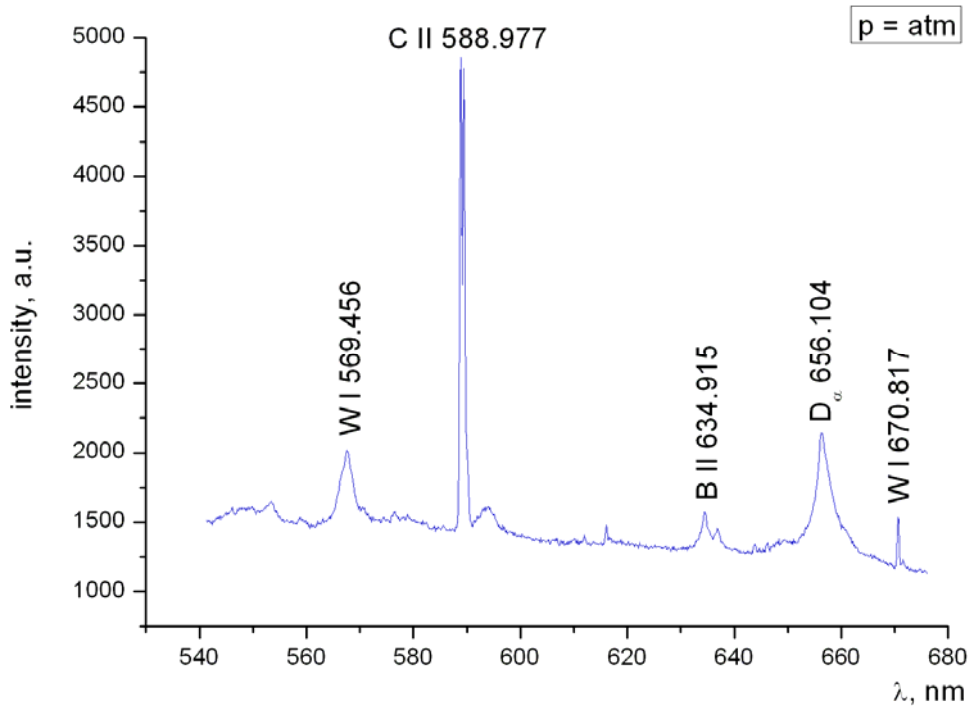


Fig.4.10 Spectra of samples taken from ASDEX Upgrade wall material [66]: a) $p=10^{-5}$ Torr, b) $p=10^{-4}$ Torr, c) $p=10^{-3}$ Torr, d) atmospheric pressure. To record each spectrum, the brightest spot of the plume was focused into the optical fibre.

The spectra taken at the pressure value of 10^{-5} Torr is the richest in lines. As the pressure increases, the number of detected spectral lines diminishes. The spectra taken in the atmospheric pressure show the least amount of the spectral lines, but their relative intensities are increased a lot compared to those recorded at lower pressures. Figure 4.11 illustrates this fact.

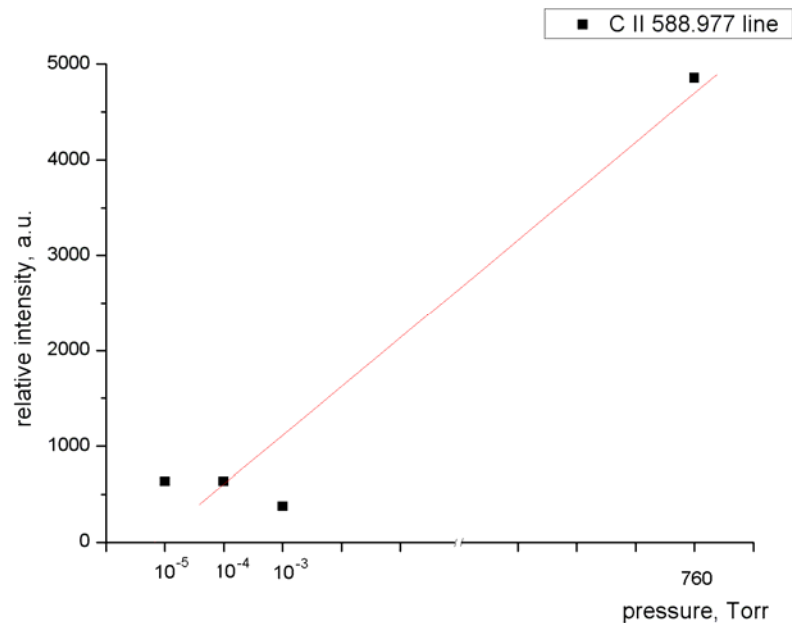


Fig.4.11 Intensity of the C II 588.977 spectral line versus pressure in a chamber at the time of recording. Chosen C II line exhibits the maximum intensity when recorded at the atmospheric pressure.

This observation may be explained with the models of propagation of laser-induced plasma plume demonstrating the development of high pressure region at the leading edge of the plume [80, 81]. At atmospheric pressure, laser-induced plasma is confined at the region next to the surface of the ablated material. The front edge of the ablation plume interacts with the background gas species, resulting in elevated brightness of the plume in the imaging point.

Plasma expansion to an ambient atmosphere can also be described in a following way [82 – 84]. The particles released from the target have a half maxwellian velocity distribution – they can move only forward. The full maxwellian distribution is reached after a limited number of collisions between particles in the Knudsen layer which has a thickness of a few mean free paths. Then the process can be described in terms of gas dynamics. The rarefaction wave propagates from the border of the expanding gas back to the target, reflects there and then the reflected rarefaction wave propagates outward. In the case of expansion into free vacuum, the rarefaction wave finally disappears with time. In the presence of an ambient gas, the plume acts like a piston ahead of which the ambient gas is compressed and heated in the external shock wave. The mass gathered ahead of the contact surface decelerates the plume. Simultaneously, the ambient gas heats the plume up to a higher temperature. The pressure grows near the contact surface and molecules of the plume collide with the ambient molecules and are reflected. An internal shock wave is formed.

The experimental observations confirm the explanations on how the relative intensity of spectral lines increases with the growth of pressure in a vacuum chamber.

Figure 4.10 also demonstrates that lower background pressure results in a lower laser energy threshold for ablation; that is why the spectra of the sample in atmospheric pressure taken under otherwise same conditions demonstrate smaller amount of detected spectral lines comparing to the rest of the spectra in the figure.

The spectrum taken at the atmospheric pressure shows broader spectral lines than in those acquired at lower pressure values. The two major line broadening mechanisms in the laser plasma are Doppler broadening and pressure broadening. The latter includes broadening by collisions with foreign species, resonance broadening and Stark broadening. Because of the low laser fluence used in the experiments, laser saturation broadening which could be caused by the probe laser in the laser atomic absorption technique can be excluded from consideration [85].

When a large number of atoms are concentrated in a small volume to produce a high density of atoms, their interactions with each other produces significant broadening of the of the emission linewidth in addition to the effect they have upon the decay time of the level causing the natural broadening of a spectral line [86]. This occurs when other atoms, ions or free electrons collide with the excited atom, and it drops down from the excited level before that electron has the opportunity for spontaneous decay.

At early times, spectral line broadening is dominated by the Stark effect due to the high initial density of free electrons and ions. Linewidths are considerably dependent on the species, being greatest for the H_α line of hydrogen at 656 nm [87]. As the plasma evolves in the post laser-pulse regime, recombination occurs, the electron density decreases, and pressure broadening (Stark effect due to near-collisions with neutrals) is often the main cause of the increasing of the linewidth. Moreover, the contribution of Van den Waals broadening begins to contribute to the linewidth appreciably when the ablation is performed at pressures approaching atmospheric [85].

Fig.4.10 demonstrates the spectra obtained after ablation of the AUG sample № IX. The concentration of deuterium measured by RBS is 4.54×10^{17} atoms/cm³, the concentration of boron - 1.37×10^{19} atoms/cm³. As in the case of previous experiments, the spectra of ASDEX Upgrade ablation targets show substantial number of impurities. Apart from tungsten and deuterium lines, Ni I (620.460 nm) is detected at pressure value of 10^{-5} Torr. The spectral line of this element might come from the stainless steel components which are not shielded from the plasma [71]. As for impurity found at 10^{-4} Torr, the both elements might appear in a spectrum. The origin of Si II (578.573 nm) line might be the material of isolation cables. Mg I (578.556 nm) can also be found among the ASDEX Upgrade impurity species [71]. The reason of appearance of B II (634.915 nm) line was explained in previous section.

The ablation rate for mentioned experimental conditions was approximately the same for and reached about 50 μm per pulse. The influence of the pressure is not significant in this case. The spectrum demonstrates the sum of the intensities of the spectral lines as the experiment was conducted to find the optimal conditions for the ablation procedure. This also explains the reason why D_α line (656.104 nm) is still present in the spectra.

The of ASDEX Upgrade samples spectra obtained at different pressure values in a vacuum chamber shows that the most feasible pressure for the ablation in vacuum using present

experimental devices is 10^{-5} Torr. The pressure does not affect, at least in detectable level, the ablation depth at used laser pulse energies. The spectrum taken at 10^{-5} Torr is well resolved and exhibits the maximal amount of lines among the other pressure values used for the investigations. The spectral lines of the impurities of interest are not subjected to the broadening as pronounced as it is in the case of the experiments at the atmospheric pressure. Moreover, the pressure of 10^{-5} Torr is easier to sustain technically during the experiments. These are the reasons why exactly this pressure is used in the further experiments.

4.2.2. Registration of the emission spectra at various distances from the target

Selective detection of the plasma light might give the possibility to enhance detection capabilities, so the strong background continuum occurring at early stages of plasma formation can be successfully reduced even without time-resolved detection [88]. It has been suggested that the separation of the plasma and the atomic emitting cloud that occurs for non-normal angles of incidence could be used to reduce the background continuum light from the laser plasma [89]. A comparison of images obtained by tuning the bandpass wavelength of the acousto-optic tunable filter on and off elemental emission lines indicates that the strong background continuum occurring at early times after plasma formation is observed from only the central part of the plasma [88].

In LIBS measurements, the plasma light is usually collected either from the central portion of the plasma by using lens imaging onto a spectrograph slit or from all portions of the plasma by using a fiber-optic bundle. In either case, the background continuum is directed into the spectrograph along with the analyte signals, and time-resolved detection is used to remove the continuum light from the measurements [90]. Because the emitting atomic cloud extends significantly beyond the volume of the most intense plasma background emissions, the possibility exists to record temporally integrated spectra that have the appearance of spectra obtained by using time-resolved detection.

Spectra of laser-induced plasma were recorded focusing fibre-optic bundle directly on ablation spark, then moving the fibre holder along the plasma plume with the step of 0.1 mm (Fig.4.12). For each step, 10 laser pulses at pulse energy of 20 mJ were accumulated.

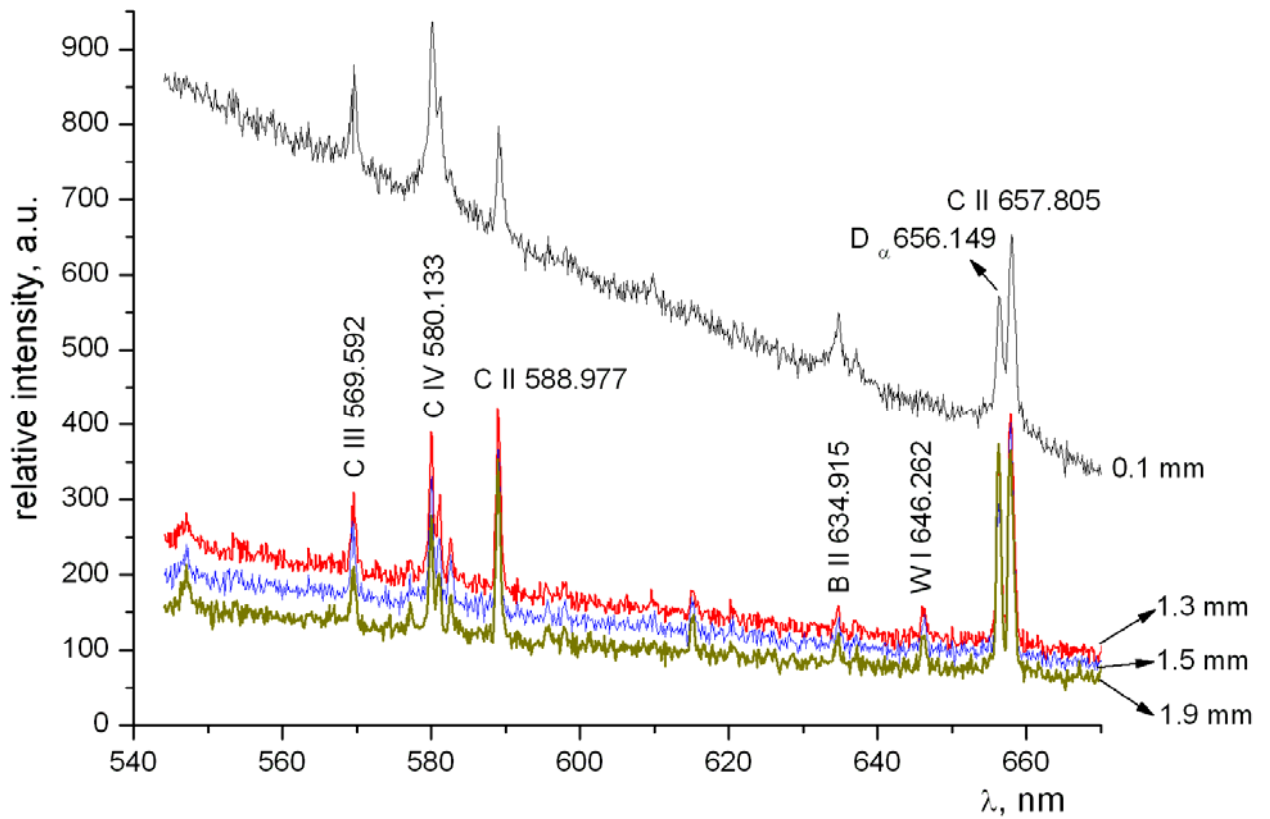


Fig.4.12. Spectra of laser-induced plasma at different distances from the ablation spark. For each spectrum, 10 pulses at energy of 20 mJ were accumulated

The tendency of decreasing of the background light with the increasing the distance from the plasma spark is clearly observed. At the distance of about 1 mm from the spark spectra exhibit similar signal-to-background ratio and spectral contents. As the optical fibre moves away from the ablated surface, the background continuum is significantly reduced compared to the spectra obtained when the brightest point of the plume is focused onto the optical fibre. The signal-to-background ratio is higher in the case when the spectra are recorded in the periphery of the ablation plume. The spectrum resembles very much a typical time-resolved LIBS spectrum with low background continuum intensity [91].

Figure 4.13 demonstrates the dependency of the intensity of CII spectral line (657.805 nm) on the distance of the point where the spectra were accumulated. The relative intensity increases and reaches its maximum at 0.3 mm from the target. Then, the decrease of the intensity is observed. This can be explained with the fact that the plasma temperature and electron densities are decreasing with increasing the distance from the ablated sample [92 – 94].

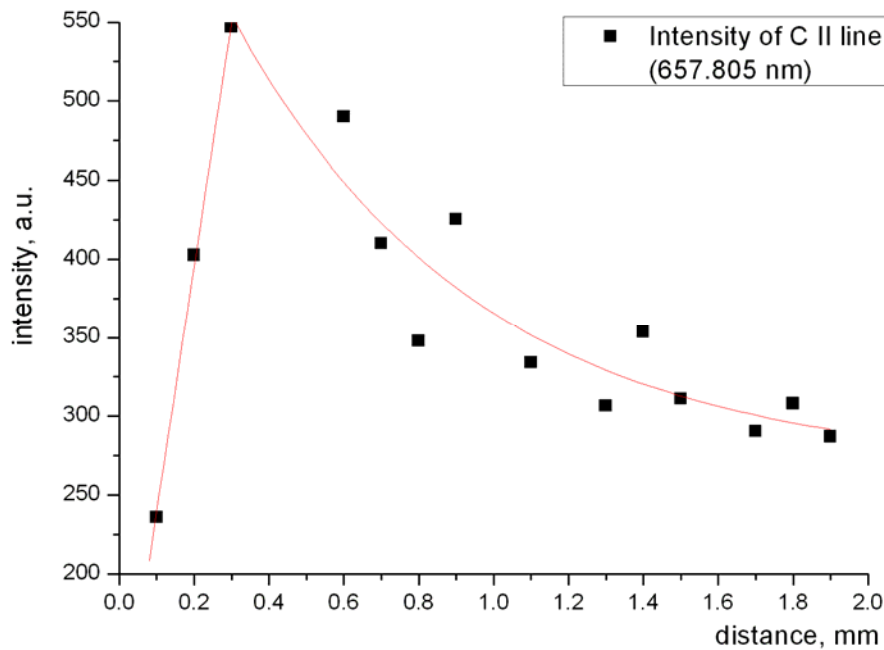


Fig.4.13. Relative intensity of CII spectral line (657.805 nm) at various distances from the ablated sample. The conditions of data accumulation are the same as in spectra in fig.4.12

As one of the potential application, accumulation of certain number of laser shots can be used for tritium desorption from plasma facing materials. Carbon materials are one of the candidates for plasma-facing materials in ITER and nuclear-fusion reactors because of its superior nature at high-heat flux and low-atomic number. However, when carbon is eroded by hydrogen plasmas containing tritium, it co-deposits with tritium, and periodical removal is required from the safety reason [95, 96].

To follow the behaviour of spectral lines in spectra, different numbers of laser pulses from 1 to 60 were applied on the surface of the sample (Fig. 4.14 a, b). The spectra were taken at the distance of 1.9 mm from the ablated target as in the periphery of the ablation plume, the spectrum resembles a time-resolved spectrum. Obtained spectra show the increase of relative intensities of carbon lines. In contrast, the signals of impurities - deuterium and boron – are decreasing with the growing number of pulses. B II 634.915 nm line is still present in the spectra obtained after 25 consecutive laser pulses, but the signal is equal to the background level in the spectra after 50 laser pulses.

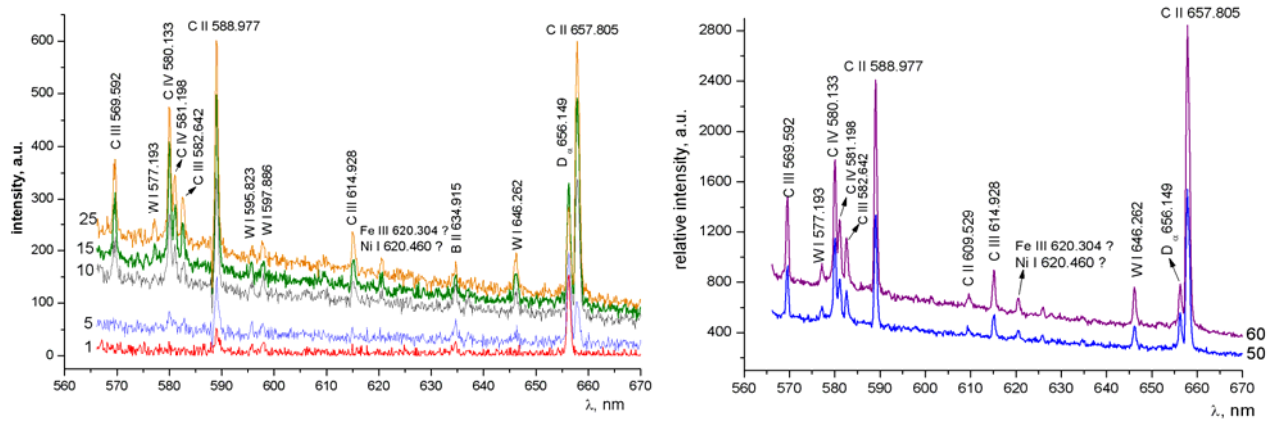


Fig.4.14 a, b. Spectra of ASDEX Upgrade sample after applying different numbers of laser pulses to the target. The numbers correspond to the amount of the applies pulses [67]

Together with laser ablation measurements, ion energy analysis can be performed [97 - 99]. Measuring ion signals before and after laser ablation, a minimal amount of laser pulses can be found to remove deuterium of tritium form the co-deposited layer completely [100]. An optimal laser treatment regime can be found, so that spectral information of other impurities can be achieved simultaneously with the process of detritiation.

The spectral composition of the samples in this chapter is similar to this described in the Chapter 4.1. The sources of the impurities are the same as described previously.

4.2.3. Ablation at different pulse energies. Depth profiles

To record the spectral information and the depth profiling of the impurities in the ASDEX Upgrade samples - deuterium and boron – certain amount of consecutive laser pulses at different pulse energy were applied on the same spot of the target. The spectra were recorded after each applied pulse. As a result, each set of spectra for certain laser pulse energy comprises as much spectra as the amount of applied pulses. All the measurements were performed at the pressure of 10^{-5} Torr. The spectra are represented in fig. 4.15.

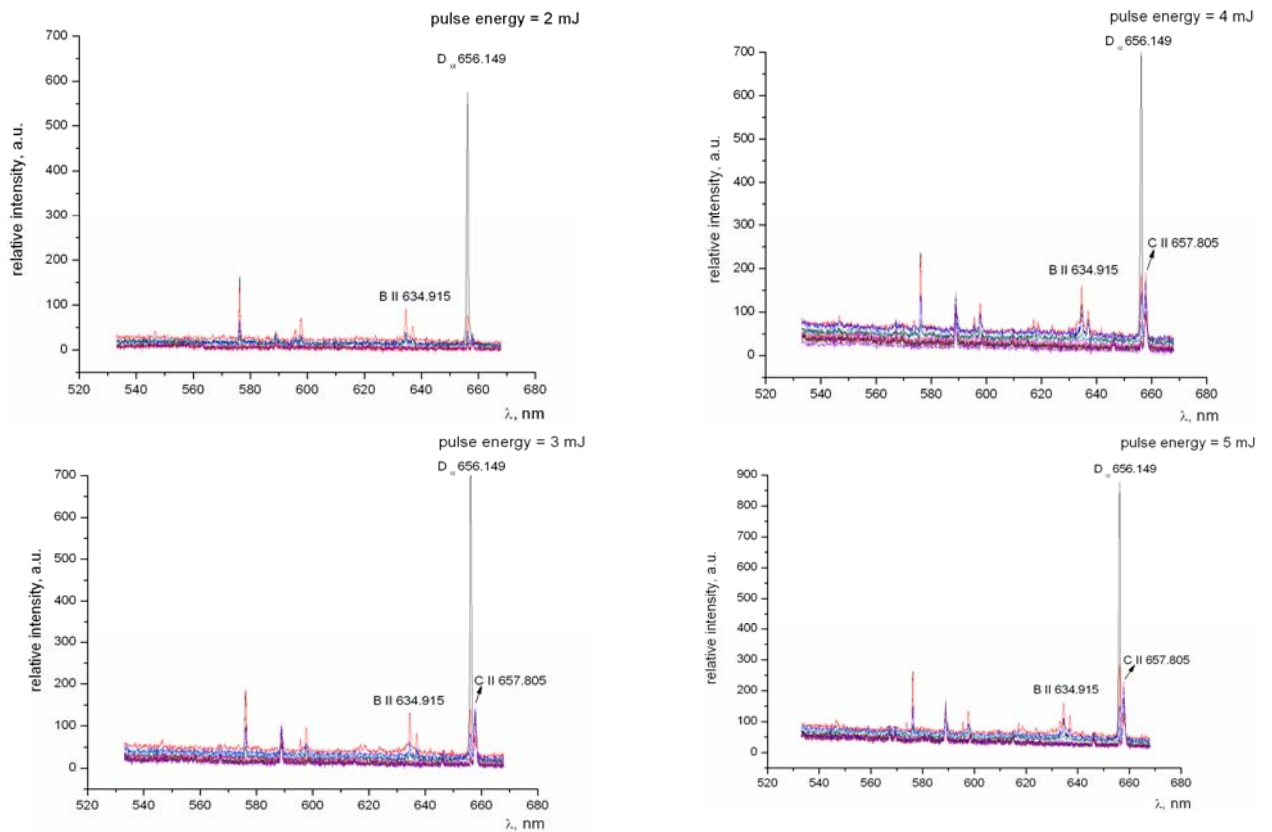


Fig.4.15. Spectra of AUG divertor material samples. 9 (in case of 2mJ pulse) to 14 (in all other cases) consecutive laser pulses were applied at the same spot of the sample. Pulse energy is indicated on each graph. Measurements were performed at the pressure of 10⁻⁵ Torr

The spectral content is not much different from the considered in the previous chapters, although the spectra recorded at low laser fluences do not exhibit such variety of impurities observed during the experiments with higher laser pulse energies. The spectra corresponding to the pulse of 2 mJ does not show C II lines (588.977 nm and 657.805 nm) which appears in the rest of the spectra recorded using higher laser fluences. This is because the fluence was 3.2 J/cm², and the ablation threshold for the graphite, which is reported to be about 3 mJ/cm² [101, 102], has barely been exceeded. In the case of pulse energy of 3 mJ, the fluence was 4.6 J/cm². This is definitely above the ablation threshold of graphite, and both lines can be detected.

Concerning depth profiles of the impurities, the relevant curves are represented in the figures 4.16 – 4.18.

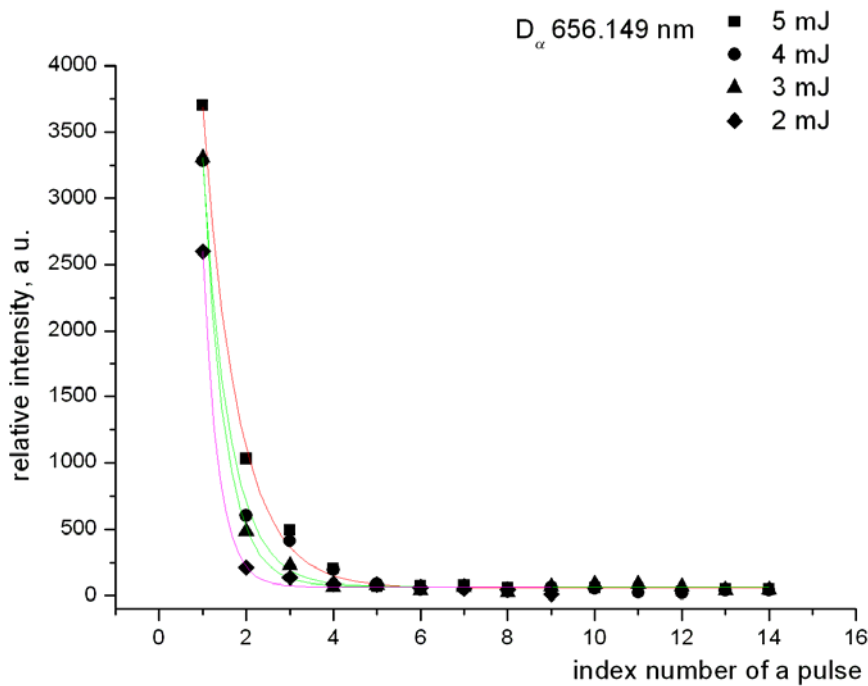


Fig. 4.16. Depth profiles of D_{α} line ($\lambda = 656.149$ nm) at different energy of a laser pulse. The pulses were applied one by one at the same spot of the sample, and the spectra recorded after each pulse. The index number of the pulse in the sequence is shown on X axis. Data are fitted exponentially.

The behaviour of D_{α} line ($\lambda = 656.149$ nm) is quite similar to one showed during the experiments at atmospheric pressure. Appearing after the 1st laser pulse and showing the maximal intensity, the sharp decrease of deuterium signal with the growing of the number of applied pulses is observed. Figure 4.15 demonstrates that after applying the 2nd laser pulse the intensity of D_{α} line has decreased almost six times compared to that after the 1st pulse. The signal of deuterium line becomes practically equal to the background level after applying the 4th laser pulse.

The evolution of the intensity of B II 634.915 nm line is depicted in figure 4.17. In contrast to the intensity of deuterium line, the maximum has been reached after the second laser pulse, but for the ablation at 5 mJ – the third pulse – was applied to the AUG target. With the fourth pulse, the intensity of the B II 634.915 nm line has decreased 5 times in comparison to the second pulse, and after the fifth pulse is practically equal to the background level.

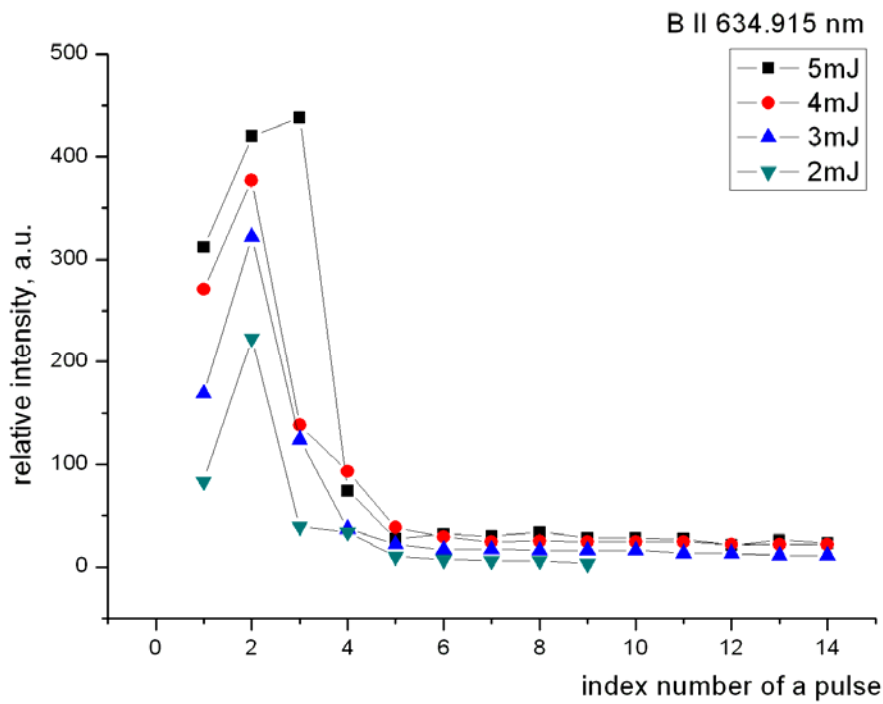


Fig. 4.17. Depth profiles of B II line ($\lambda = 634.915$ nm) at different energy of a laser pulse. The pulses were applied one by one at the same spot of the sample, and the spectra recorded after each pulse. The number of the pulse in the sequence is shown on X axis.

As for the C II 657.805 nm line, the intensity dependence on the number of laser pulses applied to the target is completely different (fig. 4.18).

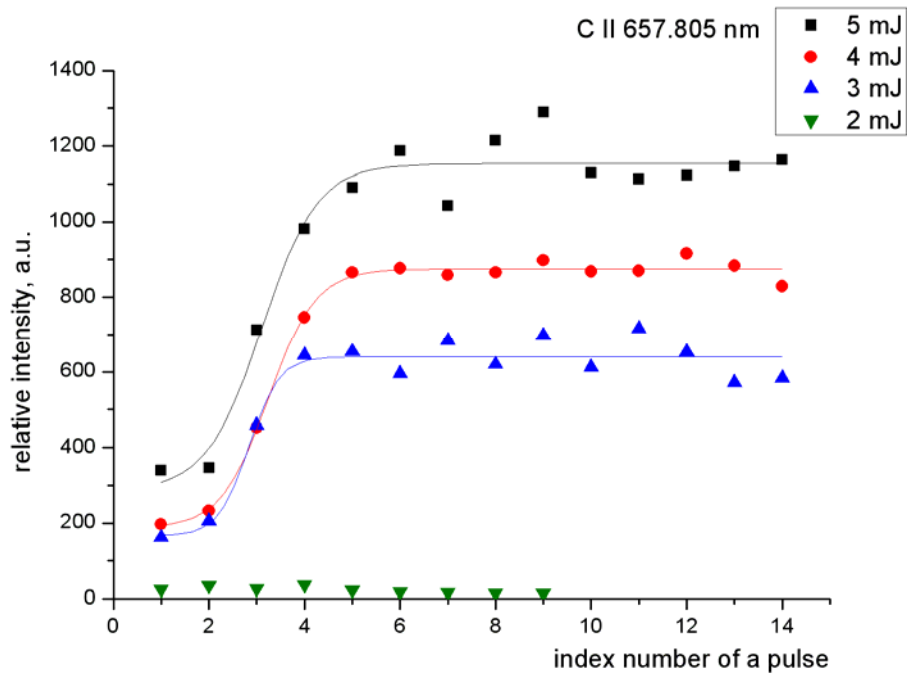


Fig.4.18. Evolution of C II line ($\lambda = 657.805$ nm) with the number of applied pulse at different pulse energy. The pulses were applied one by one at the same spot of the sample, and the spectra recorded after each pulse. The number of the pulse in the sequence is shown on X axis.

As graphite is the basic material of the ASDEX Upgrade samples, the intensity of C II 657.805 nm line is growing with the number of applied pulses, and after the 5th pulse the signal remains approximately constant. The intensities corresponding to the ablation at pulse energy of 2 mJ are nearly constant and are equal to the background level as ablation threshold for the graphite exceeded very little.

The amount of the impurities could be increased with the increasing the energy of the applied laser pulse, which, as a result, would increase the temperature of laser-induced plasma. However, the investigations of the shape of the ablation craters showed that pulse energy of 5 mJ is the optimal one for the present samples and equipment.

To investigate the shape of the ablation craters, as well as the ablation rate in case of each laser pulse energy corresponding to those used in this experiment, 100 pulses were applied on the surface of the ASDEX Upgrade tile, and then measured by the profilometer. The ablation pits for the relevant pulse energies are represented in fig. 4.19.

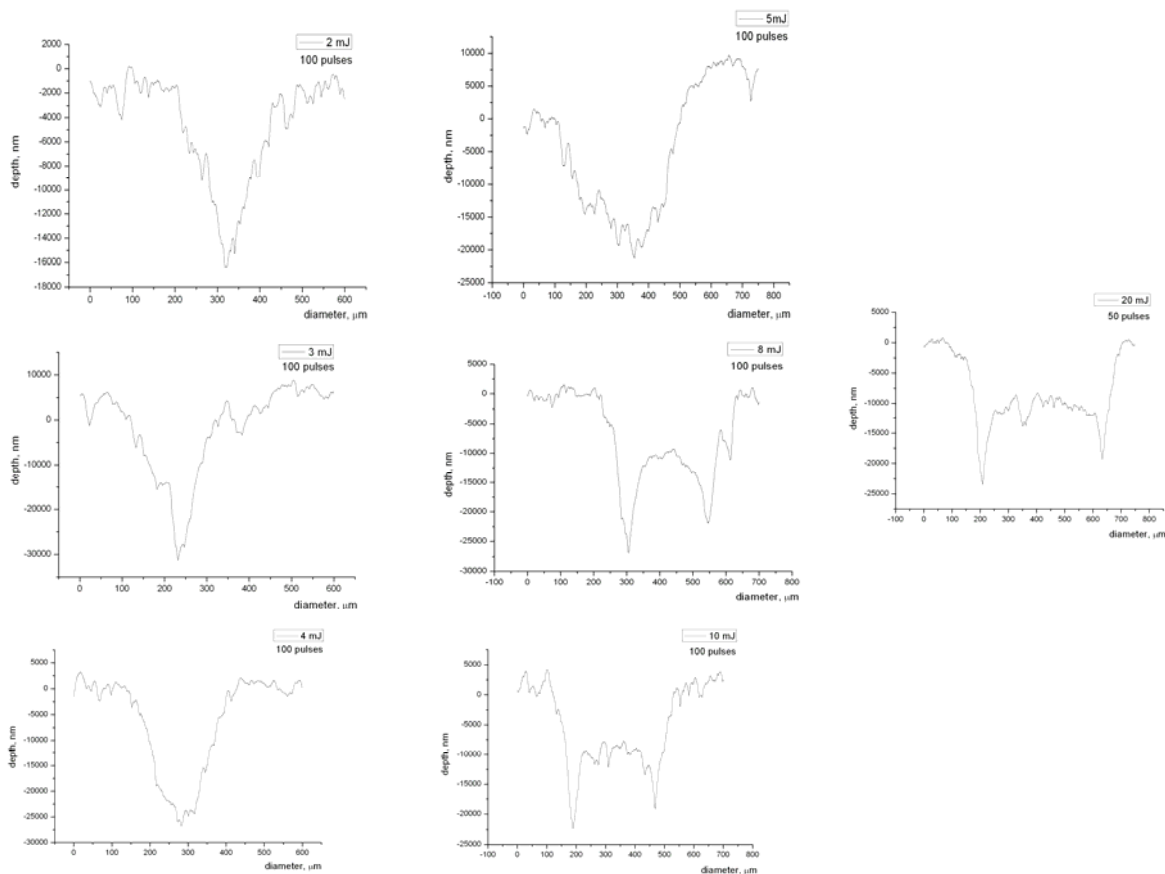


Fig. 4.19. Profiles of ablated craters. Pulse energies and accumulated shots are indicated on each graph

The profiles of the craters show that with the growth of the energy of a laser pulse, the laser profile changes dramatically. Some low-order modes start to appear, and after reaching 5 mJ in a pulse, the depth profile measurements cannot be accurate any more. Pulse shaping can improve the quality of the pits.

Figures 4.16-4.18. demonstrate the spectra obtained after ablation of the AUG sample № X. The concentration of deuterium measured by RBS is 5.84×10^{17} atoms/cm³, the concentration of boron - 1.11×10^{19} atoms/cm³. Considering the ablation removal rate in case of applying 2 -5 mJ, the results correspond to those obtained during the measurements at atmospheric pressure. Almost all the deuterium found in the ASDEX upgrade samples is released from the depth of 0.5-1 μm inside the bulk material. The concentration of boron is maximal 1 μm in the surface, and then the concentration decreases.

The depth of the craters does not exhibit considerable changes with the growth of the pulse energy, though the diameter changes significantly.

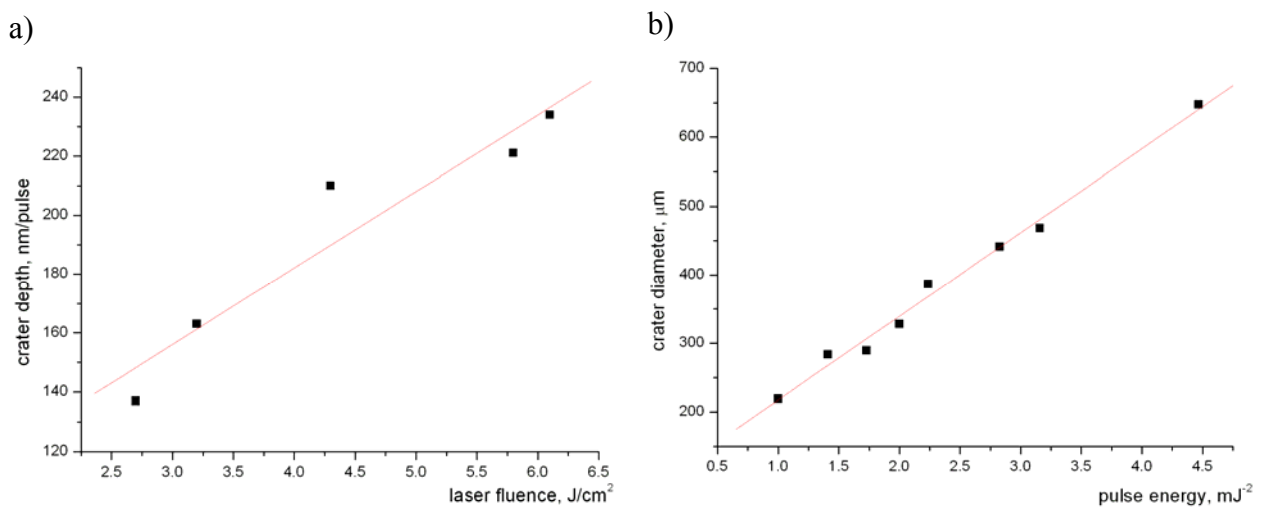


Fig. 4.20 a, b. The amount of ablated matter changes with the pulse energy of a laser beam. Crater depth (a) plotted as a function of laser fluence, and crater diameter (b) - as a function of square root of pulse energy.

As in the fluence dependence of the crater depth, the discontinuity in the crater volume data is observed in the low fluence regime, although it is not as pronounced. The discontinuity in the fluence dependence of the crater depth and crater volume, hence the onset of significant material removal, was associated with the ablation threshold.

The growth of the diameter of ablation crater scales as a square root of the pulse energy. The reason is most likely the mass transport. As the fluence is increased, a significantly larger volume of material is melted. Tight focusing leads to steep temperature gradients in the lateral dimensions, and due to the possibility of hydrodynamic flow [103], the final surface morphology is not expected to be an accurate representation of the local fluence.

Besides the shape of the ablation craters, one more aspect why the depth profiling can not be very precise is the surface of the sample itself. Figure 4.21 shows the intact surface of the ASDEX Upgrade sample scanned by means of profilometer.

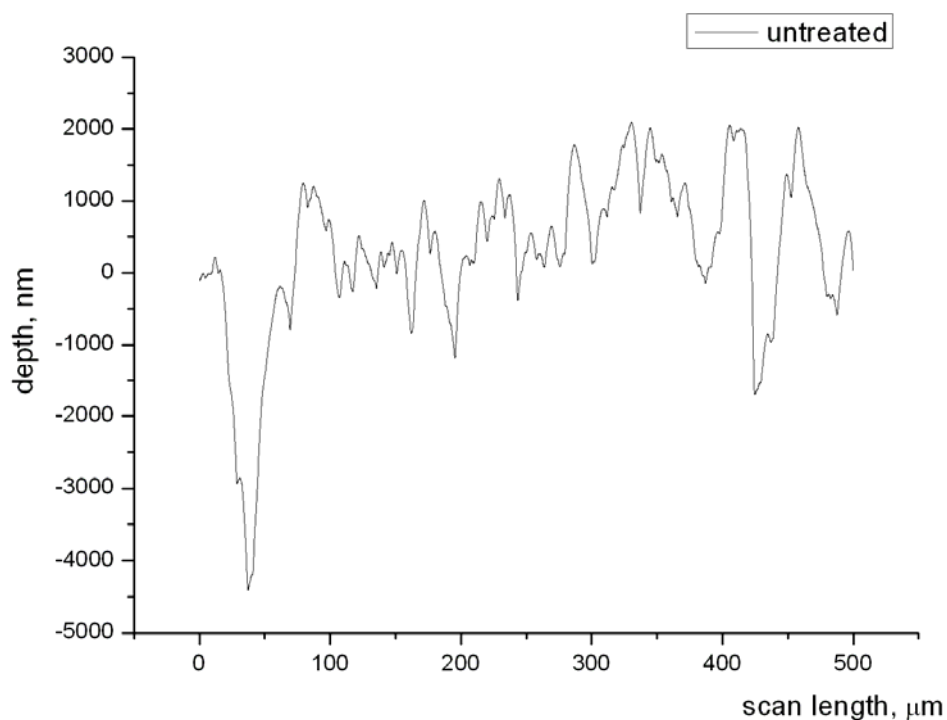


Fig. 4.21. The surface of the AUG sample not treated by the laser ablation

The sample was not treated by the laser. The scan shows relatively deep pores which can prevent the accurate analysis of the depth of the ablation craters. The erosion of the plasma facing materials inside the tokamak contributes a lot to the modification of their surface, but the specification of the R 6710 graphite shows that the material is relatively porous, and individual pores can reach $0.6 \mu\text{m}$ (see Appendix 2).

Theses

1. As an optimal pressure regime, its value in the vacuum chamber should not exceed 10^{-5} Torr since it is technically easier to sustain; line broadening at this regime is reduced; the amount of observed spectral lines of different chemical elements is maximal.
2. Signal-to-noise ratio is maximal when the spectrum is registered at 1.9 ± 0.1 mm from the ablated sample.
3. Optimal laser fluence for depth profiling is 4.3 J/cm^2 using 0.1 ns long laser pulse irrespective of laser pulse energy. If the fluence is higher, laser beam profile does not allow obtaining precise information on the depth of ablation crater.
4. Hydrogen accumulation mainly occurs at the surface layer of plasma facing components (carbon tiles) in the depth of $1 \pm 0.5 \text{ }\mu\text{m}$, which is comparable to the roughness of the carbon tile ($0.6 \text{ }\mu\text{m}$).

Conclusions and perspectives

The main results obtained in this investigation are:

- the experimental equipment for the laser induced breakdown spectroscopy analysis of the plasma facing materials has been developed on the basis of the Optical spectroscopy laboratory at the Institute of Solid State Physics;
- the methodology of the laser ablation of impurity depth profiling has been developed.

Laser-induced plasma emission spectra of the ASDEX Upgrade divertor samples were obtained using a Nd:YAG 1064 nm laser with pulse length of 150 ps and repetition rate of 10 Hz. The spectrum of the ASDEX Upgrade sample shows a substantial number of impurities. Several tungsten lines were detected as tungsten is a main material for first wall the coverage in ASDEX Upgrade. The boron left in the plasma facing material after the process of surface conditioning has been detected. The source of Fe I 390.294 nm and Ni IV 444.519 nm might be stainless steel components which are not shielded from the plasma, mainly at the outer main chamber wall and additionally the outer covering of electric cables.

As the spectrum taken at the atmospheric pressure shows broader spectral lines than in these acquired at lower pressure values, laser ablation at different pressure values has been performed. The spectra taken at the pressure value of 10^{-5} Torr is the richest in lines. As the pressure increases, the number of detected impurities diminishes. The spectra taken at the atmospheric pressure show the least amount of the spectral lines, but their relative intensities are increased a lot compared to those recorded at lower pressures. This increase of the intensity can be explained as follows. At atmospheric pressure, laser-induced plasma is confined at the region next to the surface of the ablated material. The front edge of the ablation plume interacts with the background gas species, resulting in elevated brightness of the plume in the imaging point.

The spectrum taken at 10^{-5} Torr is well resolved and exhibits the maximal amount of lines among the other pressure values used for the investigations. The spectral lines of the impurities of interest are not subjected to the broadening as pronounced as it is in the case of the experiments at the atmospheric pressure. Moreover, the pressure of 10^{-5} Torr is easier to sustain technically during the experiments.

The ablation removal rate is very similar both in experiments at atmospheric pressure and in vacuum. Applying laser pulses of 2 -5 mJ, the removal rate is around 470 nm. Almost all the

deuterium found in the ASDEX upgrade samples is released from the depth of 0.5-1 μm inside the bulk material. The boron is mostly released after applying the second pulse, which corresponds to the depth of 1-1.5 μm . This allows concluding that all deuterium is situated at the very surface of the sample, while boron is located deeper in the bulk material.

The selective detection of plasma emissions through spatial masking demonstrated the feasibility of obtaining spectra that resemble those acquired by using time-resolved detection but without using the expensive gated and intensified array detection systems required for time resolved measurements. The use of non-gated array detectors can significantly reduce the cost of a detection system given the current costs of ICCD and IPDA detectors. This result has potential application in the construction of less expensive experimental LIBS apparatus and portable LIBS instruments [88], which could be taken in to account if to consider the method of laser ablation as an in-situ technique of inspection the status of plasma facing materials inside the tokamak [104].

The tendency of decreasing of the background light with the increasing the distance from the plasma spark is clearly observed. At the distance of about 1 mm from the spark spectra exhibit similar signal-to-background ratio and spectral contents. As the optical fibre moves away from the ablated surface, the background continuum is significantly reduced compared to the spectra obtained when the brightest point of the plume is focused onto the optical fibre. The signal-to-background ration is higher in the case when the spectra are recorded in the periphery of the ablation plume. The spectrum resembles very much a typical time-resolved LIBS spectrum with low background continuum intensity. That is why for the recording of spectral information the optimal distance from the ablated target is deduced to be 1.9 mm.

The investigations of the depth profiles of the ASDEX Upgrade samples were performed at different pulse energies. Laser pulse energy of 5 mJ is considered to be the optimal pulse energy to perform laser-induced ablation spectroscopy, as with the increase of the pulse energy, some low-order modes start to appear. After reaching 5 mJ in a pulse, the depth profile measurements cannot be accurate any more.

The depth profiling of the impurities was investigated. It was shown that deuterium feature disappears after the 4th laser pulse applied to the sample, and then the intensity of the deuterium signal is practically equal to the background level. This can be improved without increasing the intensity of the laser beam applied to the target. A dual-pulse laser ablation can be used.

It was reported that multiple-pulse LIBS can yield greatly enhanced emission signals, along with improved signal-to-noise and signal-to-background ratios [105–107]. Several investigators have used multiple collinear pulses for LIBS and report enhanced emission in a variety of samples and sample matrices [105, 106]. In the dual-pulse LIBS, the air above a sample is ionized with a laser pulse focused parallel to and millimetres above the sample surface. Several microseconds later, a second pulse focused on the sample ablates material and generates laser-induced plasma in the region previously occupied by the air plasma [108].

During the double-pulse excitation experiments the first pulse generates a plasma plume. The second pulse, after a certain time delay, re-excites the plasma. Due to short delay time between the first and second pulse two separate lasers are required. Improvement of the limit of detection under double-pulse excitation showed nearly an order of magnitude compared with that in the single-pulse is reported [109].

The sensitivity of the method can be raised by replacing a CCD camera with an ICCD detector. Because the principal sensitivity limit is due to the statistical variations of number of emitted photons in terms of corresponding spatial and temporal evolution of laser plasma plume, the photo-detector should be able to resolve single photon events. The sensitivity of CCD cameras widely used as area photo-detectors in absorption and emission spectrographs has quantum efficiency close to 1. However, the sensitivity is restricted by order of 100 due the noises of analogue-digital converter. Extended intensified CCD camera (ICCD) can resolve the mentioned problem and represents an area photo-sensor with single photon sensitivity limit.

In addition to the excellent properties of the ICCD camera as a single photon detector, the ICCD camera ensures measurements of emission spectra in the different positions of the plasma plume in the given time window.

The determination of concentration of the impurities in the plasma facing materials requires the concentration calibration standards. Since the material needed for such standards are too specific, they are not commercially available. That is why a cross-calibration which can provide both the qualitative and quantitative depth profiling of the impurities is needed. Secondary ion mass spectrometry can be a good candidate for such calibration as it provides a good SIMS gives an acceptable depth resolution, which allows information on the regularity of the layer system over the structure of the sample [110, 111].

References

- [1] Th.G. Spiro, W.M. Stigliani, Eds. “Environmental Issues in Chemical Perspective”, SUNY Press, New York (1980)
- [2] R.S. Pease, Chapter 18 in “Plasma Physics. An Introductory Course”, Ed. R.Dendy, Cambridge University Press, UK (1993)
- [3] M. Yorozu, T. Yanagida, T. Nakajyo, Y. Okada, A. Endo: Laser microprobe and resonant laser ablation for depth profile measurements of hydrogen isotope atoms contained in graphite, *Appl. Opt.* 40 (2001) 2043-2046
- [4] K. Krieger, A. Geier, X. Gong, H. Maier, R. Neu, V. Rohde, ASDEX Upgrade Team: Erosion and migration of tungsten employed at the main chamber first wall of ASDEX Upgrade, *J. Nucl. Mater.* 313–316 (2003) 327–332
- [5] B. Thestrup, B. Toftmann, J. Schou, B. Doggett, J.G. Lunney: Ion dynamics in laser ablation plumes from selected metals at 355 nm, *Appl. Surf. Sci.* 197-198 (2002) 175-180
- [6] R. McWilliams, J.P. Booth, E.A. Hudson, J. Thomas, D. Zimmerman: Laser-induced fluorescence ion diagnostics in light of plasma processing, *Thin Solid Films* 515 (2007) 4860-4863
- [7] A. Tabasso, G.F. Counsell, D. Hole, J. P. Coad: Observations of hydrocarbon film deposition in the MAST tokamak, *J. Nucl. Mater.* 306 (2002), 73–77
- [8] W. Jacob, B. Landkammer, C.H. Wu: Removal of co-deposited layers by ECR discharge cleaning, *J. Nucl. Mater.* 266-269 (1999) 552-556
- [9] M. Miyamoto, K. Tokunaga, T. Fujiwara, N. Yoshida, TRIAM group, Y. Morimoto, T. Sugiyama, K. Okuno: Material properties of co-deposition formed on plasma facing materials in all-metal machine TRIAM-1M, *J. Nucl. Mater.* 313–316 (2003) 82–86

- [10] R. Sanginés de Castro, H. Sobral, C. Sánchez-Aké, M. Villagrán-Muniz: Two-colour interferometry and fast photography measurements of dual-pulsed laser ablation on graphite targets, *Phys. Lett. A* 357 (2006) 351-354
- [11] K. Krieger, W. Jacob, D.L. Rudakov, R. Bastasz, G. Federici, A. Litnovsky, H. Maier, V. Rohde, G. Strohmayer, W.P. West, J. Whaley, C.P.C. Wong, The ASDEX Upgrade and DIII-D Teams: Formation of deuterium-carbon inventories in gaps of plasma facing components, *J. Nucl. Mater.* 363-365 (2007) 870-876
- [12] A. Litnovsky, V. Philipps, A. Kirschner, P. Wienhold, G. Sergienko, A. Kreter, U. Samm, O. Schmitz, K. Krieger, P. Karduck, M. Blome, B. Emmoth, M. Rubel, U. Breuer, A. Scholl: Carbon transport, deposition and fuel accumulation in castellated structures exposed in TEXTOR, *J. Nucl. Mater.* 367-370 (2007) 1481-1486
- [13] G.M. Weyl, Chapter 1 in “Laser-induced Plasmas and Applications”, Eds. L.J Radziemski and D.A. Cremers, Marcel Dekker, New York (1989)
- [14] D.B. Chrisey, G.K. Hubler, Eds. “Pulsed Laser Deposition of Thin Films”, Wiley-Interscience, New York (1994)
- [15] Ch. Boulmer-Leborgne, J. Hermann, B. Dubreuil: Plasma formation resulting from the interaction of a laser beam with a solid metal target in an ambient gas, *Plasma Sources Sci. Technol.* 2 (1993) 219-223
- [16] J. C. Miller, R. F. Haglund, Eds.: *Laser Ablation and Desorption*, Academic Press, San Diego (1998)
- [17] R. Kelly, A. Miotello: Comments on explosive mechanisms of laser sputtering, *Appl Surf Sci* 96-98 (1996) 205-215
- [18] A. Vertes, R. W. Dreyfus, D. E. Platt: Modeling the thermal-to-plasma transitions for Cu photoablation, *IBM Journal of Research and Development*, 38 (1994) 3-10

- [19] A. Miotello, R. Kelly: Laser-induced phase explosion: new physical problems when a condensed phase approaches the thermodynamic critical temperature, *Appl. Phys. A* 69 (1999) [suppl. 1] 67
- [20] N.M. Bulgakova, A.V. Bulgakov: Pulsed laser ablation of solids: transition from normal vaporization to phase explosion, *Appl. Phys. A*, 73 (2001) 199-203
- [21] R.G. Root, Chapter 2 in “Laser-induced Plasmas and Applications”, Eds. L.J Radziemski and D.A. Cremers, Marcel Dekker, New York (1989)
- [22] R. Kelly and A. Miotello, Chapter 3 in “Pulsed Laser Deposition of Thin Films”, Eds. D.B. Chrisey and G.K. Hubler, Wiley-Interscience, New York (1994)
- [23] Y.W.Kim, Chapter 8 in “Laser-induced Plasmas and Applications”, Eds. L.J Radziemski and D.A. Cremers, Marcel Dekker, New York (1989)
- [25] S.S. Harilal, C.V Bindhu, M.S. Tillack, F. Najmabadi, A.C. Gaeris: Internal structure and expansion dynamics of laser ablation plumes into ambient gases, *J. Appl. Phys.* 93 (2003) 2380-2388
- [25] K.L. Saenger, Chapter 7 in “Pulsed Laser Deposition of Thin Films”, Eds. D.B. Chrisey and G.K. Hubler, Wiley-Interscience, New York (1994)
- [26] K.Krieger, Chapter 11 in “IPP Summer University for Plasma Physics“, Eds. M. Hirsch and H.W. Müller, Max-Planck Institut Für Plasmaphysik, Garching, Germany (2006)
- [27] G.McCracken, Chapter 16 in “Plasma Physics. An Introductory Course”, Ed. R.Dendy, Cambridge University Press, UK (1993)
- [28] V.Rohde, R.Dux, A.Kallenbach, K.Krieger, R.Neu, ASDEX Upgrade Team: Wall conditioning in ASDEX Upgrade, *J. Nucl. Mater.*, 363–365 (2007) 1369-1374
- [29] U.Schneider, W.Poschenrieder, M.Bessenrodt-Weberpals, J.Hofmann, A.Kalienbach, K.Krieger, E.Müller, H.Niedermeyer, F.Ryter, J.Roth, F.Söldner, A.Stäbler, K.H.Steuer,

O.Vollmer, F.Wagner, The ASDEX Team, The ICRH Team, The LH Team, The NI Team, The PSI Group: Boronization of ASDEX, *Journal of Nuclear Materials* 176 – 177(1990) 350-356

[30] R. Fabbro, E. Fabre, F. Amiranoff, C. Garban-Labaune, J. Virmont, M. Weinfeld, C.E. Max: Laser wavelength dependence of mass ablation rate and heat flux inhibition in laser produced plasmas, *Phys. Rev. E* 26 (1982) 2289-2292

[30] K. Watanabe, T. Iguchi: Modelling of vaporization processes of resonant laser ablation, *Appl. Phys. A* 69 (1999) S845–S848

[31] T.Q. Qiu, C.L. Tien: Heat transfer mechanisms during short-pulse laser heating of metals, *J. Heat Transfer* 115 (1993) 835–841

[32] X. Wu, M. Sadeghi, A. Vertes: Molecular dynamics of matrix assisted laser desorption of leucine enkephalin guest molecules from nicotinic acid host crystal, *J. Phys. Chem.* 102 (1998) 4770–4778

[33] L.V. Zhigilei, B.J. Garrison: Microscopic mechanisms of laser ablation of organic solids in the thermal and stress confinement irradiation regimes, *J. Appl. Phys.* 88 (2000) 1281–1298

[34] R. Mendes Ribeiro, M.M.D. Ramos, A.M. Stoneham, J.M. Correia Pires: Modelling of surface evaporation by laser ablation, *Appl. Surf. Sci.* 109–110 (1997) 158–161

[35] A.D. Boardman, B. Cresswell, J. Anderson: An analytical model for the laser ablation of materials, *Appl. Surf. Sci.* 96–98 (1996) 55–60

[36] B.C. Castle, K. Visser, B.W. Smith, J.D. Winefordner: Spatial and temporal dependence of lead emission in laser-induced breakdown spectroscopy, *Appl. Spectrosc.* 51 (1997) 1017-1024

[37] D.A. Rusak, B.C. Castle, B.W. Smith, J.D. Winefordner: Excitational, vibrational, and rotational temperatures in Nd:YAG and XeCl laser-induced plasmas, *Spec. Acta B* 52 (1997) 1929-1935

- [38] Y.I. Lee, K. Song, H.K. Cha, J.M. Lee, M.C. Park, G.H. Lee, J. Sneddon: Influence of atmosphere and irradiation wavelength on copper-plasma emission induced by excimer and Q-switched Nd:YAG laser ablation, *Appl. Spectrosc.* 51 (1997) 959
- [39] H. Kurniawan, K. Kagawa: Laser-induced shock wave plasma using long-pulse YAG laser, *Appl. Spectrosc.* 51 (1997) 304
- [40] H. Kurniawan, Y. Ishikawa, S. Nakajima, K. Kagawa: Characteristics of the secondary plasma induced by focusing a 10-mJ XeCl laser pulse at low pressures, *Appl. Spectrosc.* 51 (1997) 1769
- [41] L. St-Onge, M. Sabsabi, P. Cielo: Quantitative Analysis of Additives in Solid Zinc Alloys by Laser-induced Plasma Spectrometry, *J. Anal. At. Spectrom.* 12 (1997) 997-1004
- [42] R. Barbini, F. Colao, R. Fantoni, A. Palucci, S. Ribezzo, H.J.L. van der Steen, M. Angelone: Semi-quantitative time-resolved LIBS measurements, *Appl. Phys. B* 65 (1997) 101-107
- [43] J.M. Vadillo, J.J. Laserna: Depth-resolved analysis of multilayered samples by laser-induced breakdown spectrometry, *J. Anal. At. Spectrom.* 12 (1997) 859-862
- [44] Y.Y. Yoon, T.S. Kim, K.S. Chung, K.Y. Lee, G.H. Lee: Application of laser induced plasma spectroscopy to the analysis of rock samples, *Analyst* 122 (1997) 1223-1227
- [45] D.W. Hahn, W.L. Flower, K.R. Hencken: Discrete particle detection and metal emissions monitoring using laser-induced breakdown spectroscopy, *Appl. Spectrosc.* 51 (1997) 1836-1844
- [46] D. Anglos, S. Couris, C. Fotakis: Laser diagnostics of painted artworks: laser-induced breakdown spectroscopy in pigment identification, *Appl. Spectrosc.* 51 (1997) 1025-1030
- [47] K. Sugiyama, T. Tanabe, K. Krieger, R. Neu, N. Bekris: Tritium distribution on plasma-facing tiles from ASDEX Upgrade, *J. Nucl. Mater.* 337–339 (2005) 634–638
- [48] K. Schmid, J. Roth: Erosion of high-Z metals with typical impurity ions, *J. Nucl. Mater.* 313–316 (2003) 302–310

- [49] U. Fantz, S. Meir, ASDEX Upgrade Team: Correlation of the intensity ratio of C₂/CH molecular bands with the flux ratio of C₂H_y/CH₄ particles, *J. Nucl. Mater.* 337–339 (2005) 1087–1091
- [50] V. Rohde, H. Maier, K. Krieger, R. Neu, J. Perchermaier: ASDEX Upgrade Team: Carbon layers in the divertor of ASDEX Upgrade, *J. Nucl. Mater.* 290–293 (2001) 317–320
- [51] O.I. Buzhinskij, V.A. Barsuk, V.G. Otroshchenko, A.V. Markin, W.P. West, D.G. Whyte: The investigation of structure, chemical composition, hydrogen isotope trapping and release processes in deposition layers on graphite sample surfaces exposed to DIII-D divertor plasma in extreme conditions, *Fusion Eng Des* 61-62 (2002) 191-195
- [52] A. Kallenbach, R. Dux, J. Harhausen, C.F. Maggi, R. Neu, T. Pütterich, V. Rohde, K. Schmid, E. Wolfrum, the ASDEX Upgrade Team, Spectroscopic investigation of carbon migration with tungsten walls in ASDEX Upgrade, *J. Nucl. Mater.* 363–365 (2007) 60–65
- [53] S. Brezinsek, A. Pospieszczyk, D. Borodin, M.F. Stamp, R. Pugno, A.G. McLean, U. Fantz, A. Manhard, A. Kallenbach, N.H. Brooks, M. Groth, Ph. Mertens, V. Philipps, U. Samm, TEXTOR, ASDEX Upgrade, DIII-D Teams and JET-EFDA Contributors: Hydrocarbon injection for quantification of chemical erosion yields in tokamaks, *J. Nucl. Mater.* 363–365 (2007) 1119–1128
- [54] J. Likonen, E. Vainonen-Ahlgren, L. Khriachtchev, J.P. Coad, M. Rubel, T. Renvall, K. Arstila, D.E. Hole, Contributors to the EFDA-JET Work programme: Structural investigation of re-deposited layers in JET, *J. Nucl. Mater.* 377 (2008) 486–491
- [55] E. Fortuna, M.J. Rubel, V. Philipps, K.J. Kurzydłowski, Ph. Mertens, M. Misrkiewicz, M. Pisarek, G. Van Oost, W. Zieliński: Properties of co-deposited layers on graphite high heat flux components at the TEXTOR tokamak, *J. Nucl. Mater.* 367–370 (2007) 1507–1511
- [56] A. Huber, V. Phillips, A. Pospieszczyk, A. Kirschner, M. Lehnen, T. Ogho, K. Ohya, M. Rubel, B. Schweer, J. Von Seggern, G. Sergienko, T. Tanabe, W. Wada: Comparison of impurity production, recycling and power deposition on carbon and tungsten limiters in TEXTOR-94, *J. Nucl. Mater.* 290–293 (2001) 276–280

- [57] A. Litnovsky, P. Wienhold, V. Philipps, G. Sergienko, O. Schmitz, A. Kirschner, A. Kreter, S. Droste, U. Samm, Ph. Mertens, A.H. Donner and TEXTOR Team, D. Rudakov, S. Allen, R. Boivin, A. McLean, P. Stangeby, W. West, C. Wong and DIII-D Team, M. Lipa, B. Schunke and Tore-Supra Team, G. De Temmerman, R. Pitts and TCV Team, A. Costley, V. Voitsenya, K. Vukolov, P. Oelhafen, M. Rubel, A. Romanyuk: Diagnostic mirrors for ITER: A material choice and the impact of erosion and deposition on their performance, *J. Nucl. Mater.* 363–365 (2007) 1395–1402
- [58] R. Fabbro, E. Fabre, F. Amiranoff, C. Garban-Labaune, J. Virmont, M. Weinfeld, C.E. Max: Laser wavelength dependence of mass ablation rate and heat flux inhibition in laser produced plasmas, *Phys. Rev. E* 26 (1982) 2289-2292
- [59] B. Polyakov, A. Petruhins, J. Butikova, A. Kuzmin, I. Tale: Some aspects of pulsed laser deposition of Si nanocrystalline films, accepted in *The European Physics Journal – Applied Physics*
- [60] O. Svelto, *Principles of Lasers*, 4th Edition, Springer, New York, 1998
- [61] EKSPLA: *Laser SL 312 Technical description and laser manual*, Vilnius, 2005
- [62] Veeco Instruments Inc: *Dektak 150 surface profiler manual*, Tuscon, 2007
- [63] V.S. Burakov, S.N. Raikov: Quantitative analysis of alloys and glasses by a calibration-free method using laser-induced breakdown spectroscopy, *Spectrochim. Acta B* 62 (2007) 217-223
- [64] J. Butikova, A. Sarakovskis, B. Polyakov, I. Tale: Laser ablation for analysis of nanoscale layers, *Journal of Physics:Conference Series*, Vol.93, 2007
- [65] R. Neu, R. Pugno, M. Balden, J.Gafert, A. Geier, A. Kallenbach, V. Rohde, ASDEX Upgrade Team: Laser ablation at the inboard side of ASDEX Upgrade, *ECA* 24B (2000) 1176-1179
- [66] J. Butikova, A. Sarakovskis, I. Tale: Laser-induced breakdown spectroscopy application for determining impurity content and depth profile in the plasma facing materials, *Conference*

Proceedings of the 13th International Conference on Fusion Reactor Materials, Nice, December 10-14, 2007

[67] Yu. Ralchenko, F-C. Jou, D.E. Kelleher, A.E. Kramida, A. Musgrove, J. Reader, W.L. Wiese, K. Olsen: NIST Atomic Spectra Database (version 3.1.3), [Online]. Available: <http://physics.nist.gov/asd3>, National Institute of Standards and Technology, Gaithersburg, MD

[68] Max-Planck Institut für Plasmaphysik, Annual Report 2007

[69] R. Neu, R. Pugno, M. Balden, J.Gafert, A. Geier, A. Kallenbach, V. Rohde, ASDEX Upgrade Team: Laser ablation at the inboard side of ASDEX Upgrade, ECA 24B (2000) 1176-1179

[70] V. Rohde, R. Dux, A. Kallenbach, K. Krieger, R. Neu, ASDEX Upgrade Team, Wall conditioning in ASDEX Upgrade, J. Nucl. Mater. 363–365 (2007) 1369

[71] W. Schustereder, K. Krieger, A. Herrmann, V. Rohde, ASDEX Upgrade Team: Discharge resolved impurity flux measurements in the edge plasma of ASDEX Upgrade by exposure of collector probes, J. Nucl. Mater. 363–365 (2007) 242–246

[72] J.P. Sharpe, D. A. Petti, H. -W. Bartels: A review of dust in fusion devices: Implications for safety and operational performance, Fusion Eng. Des. 63-64 (2002) 153-163

[73] J. Winter, G. Gebauer: Dust in magnetic confinement fusion devices and its impact on plasma operation, J. Nucl. Mater. 266–269 (1999) 228-233

[74] C. Boulmer-Leborgne, J. Hermann, B. Dubreuil: Plasma formation resulting from the interaction of a laser beam with a solid metal target in an ambient gas, Plasma Sources Sci. T. 2 (1993) 219-226

[75] S.S. Harilal: Spatial and temporal evolution of argon sparks, Appl. Optics, 39 (2004) 3931-3937

- [76] A.J. Hallock, C.M. Matthews, F. Balzer, R.N. Zare: N₂ product internal-state distributions for the steady-state reactions of NO with H₂ and NH₃ on the Pt(100) surface, *J. Phys. Chem. B* 105 (2001) 8725-8728
- [77] S.S. Hamed: Spectroscopic Determination of Excitation Temperature and Electron Density in Premixed Laminar Flame, *Egypt. J. Solids* 28 No.2 (2005) 349-354
- [78] S.M. Eggins, L.P.J. Kinsley, J.M.G. Shelley: Deposition and element fractionation processes during atmospheric pressure laser sampling for analysis by ICP-MS, *Appl. Surf. Sci.* 127-129 (1998) 278-286
- [79] J. Butikova, A. Sarakovskis, I. Tale. "Laser-induced ablation spectroscopy for deuterium detection in plasma facing components", International Baltic Sea Region conference "Functional Materials and Nanotechnologies", April 1-4, 2008, Riga, Latvia
- [80] J.N. Leboeuf, K.R. Chen, J.M. Donato, D.B. Geohegan, C.L. Liu, A.A. Puretzky, R.F. Wood: Dynamical Modelling of Laser Ablation Processes, *Appl. Surf. Sci.* 96-98 (1996) 14
- [81] K.R. Chen, J.N. Leboeuf, R.F. Wood, D.B. Geohegan, J.M. Donato, C.L. Liu, A.A. Puretzky: Laser-Solid Interactions and Dynamics of the Ablated Material, *Appl. Surf. Sci.* 96-98 (1996) 45
- [82] A. Bogaerts, Zh. Chen: Effect of laser parameters on laser ablation and laser-induced plasma formation: A numerical modelling investigation, *Spec. Acta B* 60 (2005) 1280-1307 [70] N. Arnold, J. Gruber, J. Hertz, *Appl. Phys. A* 69 (suppl.) (1999) S87
- [83] V. Margetic, T. Ban, F. Leis, K. Niemax, R. Hergenröder: Hydrodynamic expansion of a femtosecond laser produced plasma, *Spectrochim. Acta B* 58 (2003) 415-425
- [84] Я.Б. Зельдович, Ю.П. Райзер, *Физика ударных волн и высокотемпературных гидродинамических явлений*, Наука, Москва, 1966
- [85] I.B. Gornushkin, L.A. King, B.W. Smith, N. Omenetto, J.D. Winefordner: Line broadening mechanisms in the low pressure laser-induced plasma, *Spectrochim. Acta B* 54 (1999) 1207-1217

- [86] T.W. Silvfast: *Laser Fundamentals*, Cambridge University Press
- [87] A.W. Miziolek, V. Palleschi, I. Schechter: *Laser-Induced Breakdown Spectroscopy (LIBS): Fundamentals and Applications*, Cambridge University Press, 2006
- [88] R.A. Multari, L.E. Foster, D.A. Cremers, M.J. Ferris: Effect of Sampling Geometry on Elemental Emissions in Laser-Induced Breakdown Spectroscopy, *Appl. Spectrosc.* 50 (1996) 1483-1499
- [89] E. H. Piepmeier and H. V. Malmstadt: Q-switched laser energy absorption in the plume of an aluminium alloy. *Anal. Chem.* 41 (1969) 700
- [90] D.A. Cremers, L.J Radziemski, *Handbook of Laser-Induced Breakdown Spectroscopy*, Wiley-VCH, 2006
- [91] J. Butikova, A. Sarakovskis, I. Tale: Laser-induced plasma spectroscopy plasma facing materials, 35th EPS Conference on Plasma Phys. Hersonissos, 9 - 13 June 2008 ECA Vol.32, P-2.011
- [92] M. Jedynski, J. Hoffman, W. Mroz, Z. Szymanski: Plasma plume induced during ArF laser ablation of hydroxyapatite, *Appl. Surf. Sci.* (2008), doi:10.1016/j.apsusc.2008.07.070
- [93] V. Narayanan, R.K. Thareja: Emission spectroscopy of laser-ablated Si plasma related to nanoparticle formation, *Appl. Surf. Sci.* 222 (2004) 382-393
- [94] J. Hermann, C. Vivien, A.P. Carricato, C. Boulmer-Leborgne: A spectroscopic study of laser ablation plasmas from Ti, Al and C targets, *Appl. Surf. Sci.* 127–129 (1998) 645–649
- [95] D. Watanabe, Y. Sakawa, T. Shibahara, K. Sugiyama, T. Shoji, K. Yamazaki, T. Tanabe: Properties of hydrogen desorption from co-deposits on JT-60 graphite tile by pulsed-laser ablation, *J. Nucl. Mater.* 363-365 (2007) 972-976
- [96] G. Federici, R.A. Anderl, P. Andrew, J.N. Brooks, R.A. Causey, J.P. Coad, D. Cowgill, R.P. Doemer, A.A. Haasz, G. Janeschitz, W. Jacob, G.R. Longhurst, R. Nygren, A. Peacock, M.A. Pick, V. Philipps, J. Roth, C.H. Skinner, W.R. Wampler: In-vessel tritium retention and removal in ITER, *J. Nucl. Mater.* 266–269 (1999) 14-29

- [97] T. Åkermark, B. Emmoth, H. Bergsåker: Laser annealing in combination with mass spectroscopy, a technique to study deuterium on tokamak carbon samples, a tool for detritiation, *J. Nucl. Mater.* 359 (2006) 220-226
- [98] Y. Sakawa, K. Sato, T. Shibahara, T. Tanabe: Ablation of hydrogen-implanted graphite target using pulsed laser beam, *Fusion Eng. Des.* 81 (2006) 381-386
- [99] A. Huber, M. Mayer, V. Philipps, A. Pospieszczyk, T. Ohgo, M. Rubel, B. Schweer, G. Sergienko, T. Tanabe: In-situ measurement of trapped hydrogen by laser desorption in TEXTOR-94, *Phys. Scr.* T94 (2001) 102–105
- [100] P. Gąsior, J. Badziak, A. Czarnecka, P. Parys, J. Wołowski, M. Rosiński, M. Rubel, V. Philipps: Characterization of laser-irradiated co-deposited layers on plasma facing components from a tokamak, *Phys. Scr.* T123 (2006) 99–103
- [101] F. Le Guern, C. Hubert, S. Mousset, E. Gauthier, C. Blanc, P. Wodling, J.M. Weulersse: Laser ablation tests performed on TORE-SUPRA graphite samples, *J. Nucl. Mater.* 335 (2004) 410-416
- [102] H.O. Jeschke, M.E. Garcia: Theoretical description of the ultrafast ablation of diamond and graphite: dependence of thresholds on pulse duration, *Appl. Surf. Sci.* 197–198 (2002) 107–113
- [103] T.D. Bennett, D.J. Krajnovich, C.P. Grigoropoulos, P. Baumgart, A.C. Tam: Marangoni Mechanism in pulsed laser texturing of magnetic hard disks. *J. Heat Transf.* 119 (1997) 589-596
- [104] C. Grisolia, A. Semerok, J.M. Weulersse, F. Le Guern, S. Fomichev, F. Brygo, P. Fichet, P.Y. Thro, P. Coad, N. Bekris, M. Stamp, S. Rosanvallon, G. Piazza: In-situ tokamak laser applications for detritiation and co-deposited layers studies, *J. Nucl. Mater.* 363-365 (2006) 1138-1147
- [105] L. St-Onge, V. Detalle, M. Sabsabi: Enhanced laserinduced breakdown spectroscopy using the combination of fourth-harmonic and fundamental Nd:YAG laser pulses, *Spectrochim. Acta Part B* 57 (2002) 121–135

- [106] D. N. Stratis, K. L. Eland, S. M. Angel: Enhancement of aluminium, titanium, and iron in glass using pre-ablation spark dual-pulse LIBS, *Appl. Spectrosc.* 54 (2000) 1719–1726
- [107] S. M. Angel, D. N. Stratis, K. L. Eland, T. Lai, M. A. Berg, D. A. Gold: LIBS using dual- and ultra-short laser pulses, *Fresenius J. Anal. Chem.* 369 (2001) 320–327
- [108] J. Scaffidi, J. Pender, W. Pearman, S.R. Goode, B.W. Colston, Jr., J. Chance Carter, S.M. Angel: Dual-pulse laser-induced breakdown spectroscopy with combinations of femtosecond and nanosecond laser pulses, *Appl. Opt.* 42 Nr. 30 (2003) 6099-6106
- [109] A. Kumar, F.Y. Yueh, J.P. Singh: Double-pulse laser-induced breakdown spectroscopy with liquid jets of different thicknesses, *Appl. Opt.* 42 Nr. 30 (2003) 6047-6051
- [110] S. Oswald, S. Baunack: Comparison of depth profiling techniques using ion sputtering from the practical point of view, *Thin Solid Films* 425 (2003) 9–19
- [111] J.R. Shallenberger, D.A. Cole, S.W. Novak, R.L. Moore, M.J. Edgell, S.P. Smith, C.J. Hitzman, J.F. Kirchoff, E. Principe, S. Biswas, R.J. Bleiler, W. Nieveen, K. Jones,: Oxide Thickness Determination by XPS, AES, SIMS, RBS and TEM, *Proceedings of the 1998 International Conference on Ion Implantation Technology*, Vol. 1, 79-82

List of author's scientific publications

1. J. Butikova, A. Sarakovskis, B. Polyakov, I. Tale: Laser ablation for analysis of nanoscale layers, Journal of Physics:Conference Series, Vol.93, 2007
2. J. Butikova, A. Sarakovskis, I. Tale: Laser-induced breakdown spectroscopy application for determining impurity content and depth profile in the plasma facing materials, Conference Proceedings of the 13th International Conference on Fusion Reactor Materials, Nice, December 10-14, 2007
3. J. Butikova, A. Sarakovskis, I. Tale: Laser-induced ablation spectroscopy for deuterium detection in plasma facing components, submitted to Scripta Materialia
4. J. Butikova, A. Sarakovskis, I. Tale: Laser-induced plasma spectroscopy plasma facing materials, 35th EPS Conference on Plasma Phys. Hersonissos, 9 - 13 June 2008 ECA Vol.32, P-2.011

Participation in conferences

1. J. Butikova, I. Tale. "Laser Ablation Spectroscopy for Concentration of Impurity Elements", ISSP 21st Scientific Conference, Abstract Book, 2005, Riga, Latvia
2. J. Butikova, I.Tale. "Laser Ablation Spectroscopy for Impurity Depth Profiling in Plasma", Book of Abstracts of the 7th International Summer School-Conference *Advanced Materials and Technologies*. ISBN 9955-09-894-5, 2005 Aug, p.129, Palanga, Lithuania
3. J. Butikova. "Laser Ablation Spectroscopy for Impurity Depth Profiling and Concentration Imaging in Plasma", internal seminar at the Department of Material Sciences, Max Planck Institute of Plasma Physics, October 2005, Garching, Germany
4. J. Butikova. "Rutherford backscattering measurements for laser induced breakdown spectroscopy standards". ISSP 22nd Scientific Conference, Abstract Book, p. 41, 2006, Riga, Latvia
5. J. Butikova. "Laser Induced Breakdown Spectroscopy", internal seminar at the Department of Material Sciences, Max Planck Institute of Plasma Physics, October 2006, Garching, Germany
6. J. Butikova, A. Sharakovskiy, I. Tāle. "Development of Equipment for Laser Ablation Spectroscopy", ISSP 23rd Scientific Conference, Abstract Book, p. 53, 2007, Riga, Latvia
7. J. Butikova, A. Sarakovskis, I. Tale. "Laser Ablation Spectroscopy of Plasma-facing Materials", Development in Optics and Communications 2007, Abstract Book, p.15, Riga, Latvia
8. J. Butikova, A. Sarakovskis, B. Polyakov, I. Tale. "Laser ablation for analysis of nanoscale layers", International Baltic Sea Region conference "Functional Materials and Nanotechnologies", April 2-4, 2007, Riga, Latvia
9. J. Butikova, A. Sarakovskis. "Laser ablation spectroscopy for impurity depth profiling and concentration imaging in plasma", EFDA Workshop, October 2007, Riga, Latvia

10. J. Butikova, A. Sarakovskis, I. Tale. "Laser-induced breakdown spectroscopy application for determining impurity content and depth profile in the plasma facing materials", Conference Proceedings of the 13th International Conference on Fusion Reactor Materials, December 10-14, 2007, Nice, France
11. J. Butikova, A. Sarakovskis, I. Tale. "Laser ablation spectroscopy of the first wall materials of *ASDEX Upgrade* tokamak", ISSP 24th Scientific Conference, February 2008, Riga, Latvia
12. J. Butikova, A. Sarakovskis, I. Tale. "Laser-induced ablation spectroscopy for deuterium detection in plasma facing components", International Baltic Sea Region conference "Functional Materials and Nanotechnologies", April 1-4, 2008, Riga, Latvia
13. J. Butikova. "Laser-induced breakdown spectroscopy of plasma facing materials", May 28th, 2008 – invited lecture at the Faculty of Physics, Vilnius University
14. J. Butikova, A. Sarakovskis, I. Tale. "Laser-induced ablation spectroscopy of plasma facing materials", 35th EPS Conference on Plasma Physics, June 9-13, 2008, Hersonissos, Greece

Acknowledgement

Author is grateful for the supervisor Prof. Ivars Tāle for valuable discussions and practical help. Many thanks to the colleagues at the Optical spectroscopy laboratory of the Institute of Solid State Physics for discussions, technical support and nice time spent at and outside the lab.

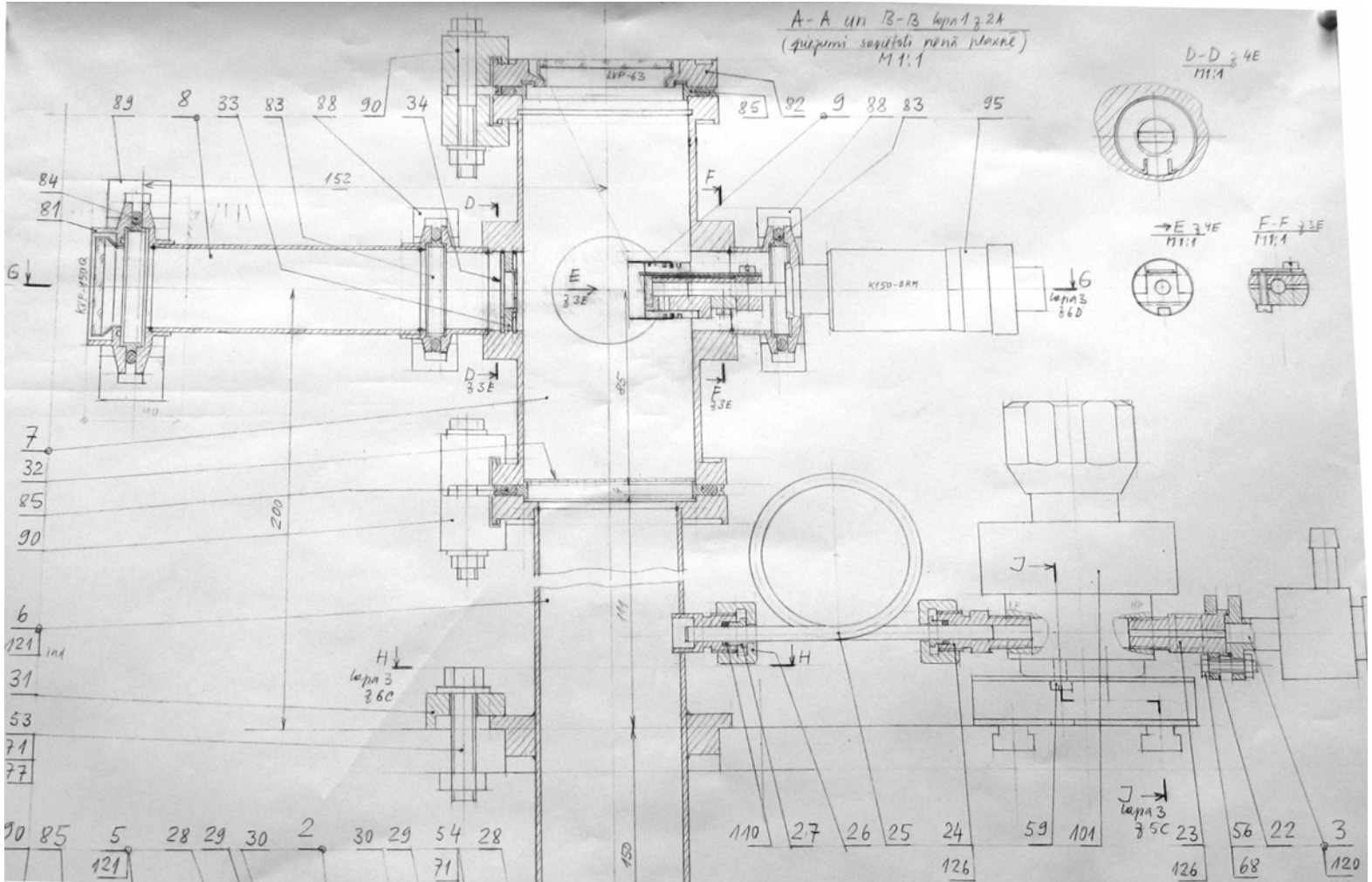
The gratitude should also be expressed to Dr. Karl Krieger at the Material Sciences divisions, Max Planck Institute of Plasma Physics for the great help in obtaining the objects of the investigation, as well as for the possibility to perform tandem accelerator measurements.

This study was supported by the European Social Fund and ATLAS (Advanced Training in Laser Sciences) project (MEST-CT-2004-008048).

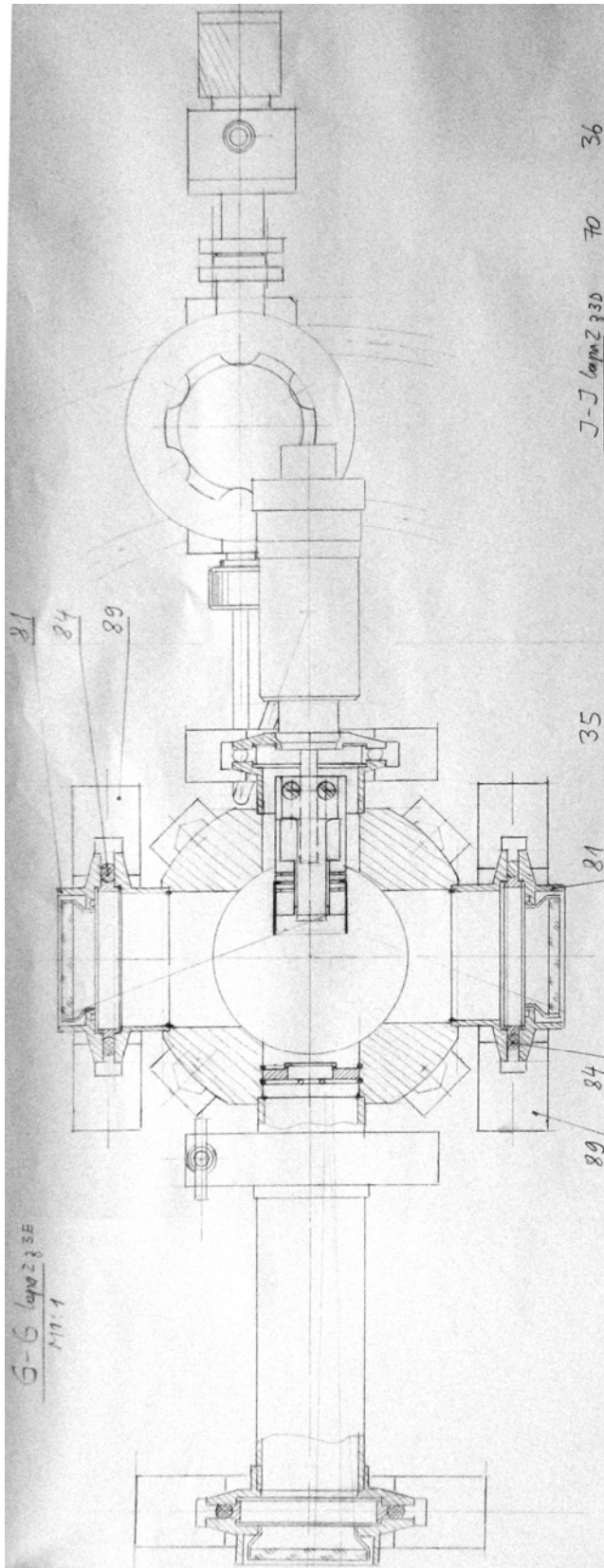



Appendix 1

a) Drawing of the vacuum chamber



b) Drawing of the vacuum chamber – view from the top



 SGL CARBON GROUP Business Area Specialty Graphite	Technische Information / Technical Information R 6710	15.11.1996
---	---	------------

Typische Werte für die Marke R 6710 / Typical Values for Grade R 6710

Werkstoff / material: Graphit / graphite
 Formgebung / forming: isostatisch gepreßt / isostatically pressed
 Einsatz / applications: Halbleiter-Technologie / semiconductor applications

Eigenschaft property	Methode test standard	Wert value	Einheit unit
mittlere Korngröße average grain size		3	μm
Dichte bulk density	DIN IEC 413 / 203	1.88	g/cm^3
Porosität porosity	DIN 66133	10	Vol. %
Porengröße pore size	DIN 66133	0.6	μm
Permeabilität permeability	DIN 51935	0.01	cm^2/s
Rockwell-Härte $\text{HR}_{5/100}$ Rockwell hardness $\text{HR}_{5/100}$	DIN IEC 413 / 303	110	
spezif. elektr. Widerstand specific electrical resistivity	DIN 51911	13	$\mu\Omega\text{m}$
Biegefestigkeit flexural strength	DIN 51902	85	N/mm^2
Druckfestigkeit compressive strength	DIN 51910	240	N/mm^2
Elastizitätsmodul Youngs modulus	DIN 51915	14	$10^3\text{N}/\text{mm}^2$
therm. Ausdehnung (20-200°C) therm. expansion (68-392°F)	DIN 51909	$4.7 \cdot 10^{-6}$	K^{-1}
Wärmeleitfähigkeit thermal conductivity	DIN 51908	100	$\text{W}\cdot\text{m}^{-1}\cdot\text{K}^{-1}$
Aschewert ash value	DIN 51903	*)	ppm

*) Asche gemäß Spezifikation
 Ash content according purity specifications

Erstellt: ZQK	Freigegeben: ZQ	Freigegeben: CEI	Blatt 1/1
---------------	-----------------	------------------	-----------